# About the zero Mach number assumption in the calculation of thermoacoustic instabilities

Franck Nicoud, Kerstin Wieczorek

# About the zero Mach number assumption in the calculation of thermoacoustic instabilities

By F. NICOUD[1] † AND K. WIECZOREK[1,2]

[1]University Montpellier II - I3M CNRS UMR 5149
Place Eugène Bataillon. 34095 Montpellier cedex 5 - France.
[2] CERFACS - 42, Av. Gaspard Coriolis, 31057 Toulouse cedex 1 - France.

(Received April 2008)

This paper presents an analytical/numerical study of the effects of the mean flow on thermo-acoustic instabilities. Simple quasi-1D configurations such as a 1D premixed flame in a duct connected to a nozzle are considered in order to investigate to what extent the frequency of oscillation and growth rate are modified when the Mach number is not zero. It is demonstrated that the zero Mach number assumption for the mean flow can lead to significant errors, especially when the mean flow is not isentropic, a condition which is always met in combustion applications. The analysis confirms that terms involving the mean velocity may contribute to the disturbance energy equation as much as the the flame forcing ('Rayleigh') term. Besides, the net effect of the non zero Mach number terms on the stability of the modes strongly depends on both the boundary conditions and the flame response. For moderate Mach number values of order 0.05, the errors made by assuming that the mean flow is at rest are large enough to change the stability of the frequencies of interest in an academic combustor.

## 1. INTRODUCTION

Thermo-acoustic instabilities, which arise from the coupling between acoustic waves and flames, can lead to high amplitude instabilities [1–4]. In general, these instabilities induce oscillations of all physical quantities (pressure, velocities, temperature, etc ...); in the most extreme cases, they can destroy the burner by inducing large amplitude flame motion (flashback) or unsteady pressure (material fatigue). Since the equivalence ratio oscillates when instabilities are present, there is a general trend for combustors to be more unstable when operating in the lean regime. Besides, due to new international constraints, pollutant emissions must be reduced and gas turbine manufacturers need to operate their systems under leaner and leaner conditions. Consequently, there is a need to better understand combustion instabilities and to be able to predict them at the *design* level [5].

Three types of methods have been considered so far to predict/describe these instabilities:

(*a*) Large Eddy Simulation (LES) of all relevant scales of the reacting, turbulent, compressible flow where the instability develops. Multiple recent papers have demonstrated the power of this method to represent the flame dynamics [6–12], as well as the interaction between the reaction zone and the acoustic waves [13–16]. However, even when they confirm that a combustor is unstable, LES calculations do not say why and how to control its instability. Besides, because of its intrinsic nature (full

† Corresponding author: franck.nicoud@univ-montp2.fr

three-dimensional resolution of the unsteady Navier-Stokes equations), LES remains very CPU demanding, even on today's computers,

($b$) Low-order methods where the geometry of the combustor is modelled by a network of homogeneous (constant density) 1D or 2D axisymmetric acoustic elements where the acoustic problem can be solved analytically [17–22]. Jump relations are used to connect all these elements, enforcing pressure continuity and flow rate conservation and accounting for the dilatation induced by the infinitely thin flame, if any. The acoustic quantities in each segment are related to the amplitudes of the forward and backward acoustic waves which are determined such that all the jump relations and the boundary conditions are satisfied. This can only be achieved for a discrete set of frequencies $\omega$ which are the roots of a dispersion relation in the complex plane. The main advantage of low-order methods is that they allow to represent a complex system with only a few parameters, thus allowing an extensive use for pre-design/optimization/control purposes. However, the geometrical details of the combustor cannot be accounted for and only the first "equivalent" longitudinal or orthoradial modes are sought for,

($c$) As an intermediate between LES and low-order methods, one may consider using a finite-element or finite volume technique to solve for an equation (or a system of equations) describing the space-time evolution of small amplitude fluctuations. A set of linear transport equations for the perturbations of velocity, temperature and density can be derived by linearizing the Navier-Stokes equations [23], where the local unsteady heat release appears as a forcing term. This term is responsible for combustion noise and thermo-acoustic instabilities and must be modeled to close the linearized set of equations. Assuming that this modeling problem can be addressed appropriately, the system of linear partial differential equations for the fluctuating quantities is closed and can be solved, for example in the time domain [24]. Depending on the coupling between the flame and acoustics, especially the phase between the pressure and heat release fluctuations, some modes present in the initial field can be amplified and grow exponentially; after a while, the unsteady field is dominated by the most amplified mode which can then be analyzed [24]. To facilitate the description of time delayed boundary conditions and also to obtain more information about the damped or less amplified mode, it is worth solving the set of linear equations in the frequency space, as proposed by Rao and Morris [25] for the wave propagation issue over a complex baseline flow. If applied within the combustion instability framework, this would give rise to an eigenvalue problem, the eigenvalues being related to the (complex valued) frequencies of the thermo-acoustic modes. Since in general viscous contributions are negligible when dealing with acoustic propagation, the appropriate set of equations to solve are the Linearized Euler Equations.

Three modes of fluctuations can perturb an otherwise steady baseline flow: acoustic waves, entropy waves and vorticity waves [26]. Acoustic perturbations propagate at the speed of sound augmented by the local mean velocity while the last two modes are simply convected by the mean flow. In general, these three types of fluctuations are coupled, even in the linear regime, making the distinction between the fluctuating modes a difficult task [27]. The linearized approach discussed above simplifies considerably if the baseline flow is assumed homentropic and irrotational since a wave equation for the perturbation potential can then be derived [28] and used in place of the Linearized Euler Equations. Since assuming the mean flow to be homentropic is obviously not justified when dealing with combustion instabilities, it is often assumed that the mean flow is at rest instead of being potential. The advantage of this more restrictive assumption on

the velocity field is that neither the entropy nor the vorticity mode can propagate so that a wave equation for the acoustic perturbations can be derived, without assuming the baseline flow is homentropic. The Linearized Euler Equations can then be replaced by a forced Helmholtz equation with variable coefficients [29]. Combined with LES, this approach proved useful to better understand the structure and nature of the instabilities observed in academic or industrial burners [15, 30, 31]. However, no clear justification of the zero Mach number assumption has been provided so far, as discussed by Keller et al. [32], Dowling [33], Polifke et al. [34, 35], Sattelmayer [36].

Actually this simplification may induce significant changes on the frequency and growth rate of the thermo-acoustic modes in at least three ways:

($a$) **acoustic boundary conditions:** when analyzing the thermo-acoustic modes of an industrial combustor (e.g.: a gas turbine), one must account for the proper acoustic environment of the combustion chamber. This means prescribing complex valued impedance at the boundaries of the computational domain. For example, if one assumes that the high pressure distributor which connects the combustor to the downstream turbine [37] is choked, one may want to impose the appropriate boundary impedance (e.g. assessed from the theory of compact isentropic nozzles [38]) at the outlet section of the computational domain. In theory the impedance should be defined in a section where the Mach number is *very small*, consistently with the zero Mach number approximation used to formulate the thermo-acoustic problem. In practice, the location of the outlet section is often imposed by geometrical considerations and the effective Mach number at the boundary is not a free parameter,

($b$) **coupling with the flame:** when a flame is present, the mean entropy field is not uniform and couples with the acoustic perturbations to generate hot spots (entropy waves). Under the zero Mach number assumption, these spots do not propagate and thus do not modify the fields of fluctuating quantities far from the reacting zone. The situation changes as soon as the baseline flow is not at rest since any entropy spots can then be convected away from the flame,

($c$) **acoustic/entropy coupling at the downstream boundary:** when the entropy waves generated in the flame region are convected downstream, they can couple with the accelerated baseline flow in the high pressure distributor (or its equivalent quasi-1D nozzle). From this interaction result acoustic waves, which can propagate upstream and eventually modify the thermo-acoustic modes. Of course, this phenomenon is not accounted for when the zero Mach number approximation is used to model the combustor because entropy waves never reach the outlet section in this case. Its implications regarding the overall thermo-acoustic stability of the system have been studied analytically by Keller et al. [32], Polifke et al. [34, 35]. In their view, an acoustic disturbance in the chamber produces a fluctuation of equivalence ratio which in turn generates a disturbance of the temperature downstream the premixed flame. Once it is convected toward the downstream (choked) nozzle, the corresponding entropy spot is partly converted into acoustics [38] and depending on the overall phase relationship, this may enhance or damp the thermo-acoustic modes of the whole system. Sattelmayer [36] added more physics by accounting for the dispersion of the entropy fluctuations during their propagation from the injector and/or the flame to the exit nozzle. Contrary to the approach of Keller et al. [32], Polifke et al. [34, 35], Sattelmayer [36], which is restricted to low speed flows, the semi-analytical description of the mean flow effects proposed by Dowling [33] is valid for arbitrary Mach numbers (see section 4.2.2). Note that all the (semi-)analytical studies rely on the assumption that the reaction zone and exit nozzle are infinitely thin.

The objective of this paper is to assess the potential errors associated with the above

mentioned issues related to the zero Mach number assumption. For doing so, several analytical results and numerical tools will be used in order to study the thermo-acoustic modes of simple configurations, including a constant cross section duct with a premixed 1D flame (1D configuration) and a constant cross section duct with or without a flame connected to a nozzle (quasi-1D configuration). The use of adapted numerical tools for solving the Linearized Euler Equations together with an energy analysis of the disturbances will allow to draw a clearer view of **a)** the change of the spatial structure of the thermo-acoustic modes when the mean flow is no longer at rest, **b)** the main contributors to the thermo-acoustic stability/instability when the Mach number is not zero. The basic equations are first given in section 2 where different levels of approximation are considered. The different numerical tools used in the paper are described in section 3 and the results are presented in section 4 for three academic configurations.

Note that another potential effect of the mean flow being not at rest is to increase the non-orthogonality of the eigenmodes. In the zero Mach number case, it has been shown by Nicoud et al. [29] that the thermoacoustic modes are not mutually orthogonal as soon as unsteady combustion occurs or finite complex valued boundary impedance is accounted for. This property and its consequences have been analyzed in detail in the case of the Rijke tube by Balasubramanian and Sujith [39], who demonstrated the relevancy of this feature to the triggering phenomenon. Since non-normality is also known to be related to convective effects in classical, incompressible fluid mechanics [40], it is the authors point of view that a side effect of accounting for non zero Mach number effects is most probably to enhance the non-orthogonality of the modes as well as its consequences in terms of triggering and bootstrapping [39, 41]. However, this issue is out of the scope of this paper which only deals with the behavior of the eigenmodes, without considering combinations of modes.

## 2. MATHEMATICAL FORMULATIONS

The purpose of this section is to give the different mathematical representations relevant to the configurations that will be considered in section 4. One considers an homogeneous reacting mixture with constant heat capacities $C_p$ and $C_v$; viscous terms (molecular diffusion of momentum and heat) are neglected in the remainder of this paper.

### 2.1. *Linearized Euler Equations*

Under the above assumptions, the mass, momentum and entropy equations read respectively:

$$\frac{D\rho}{Dt} = -\rho\nabla\cdot\mathbf{u}, \tag{2.1}$$

$$\rho\frac{D\mathbf{u}}{Dt} = -\nabla p, \tag{2.2}$$

$$\frac{Ds}{Dt} = \frac{rq}{p}, \tag{2.3}$$

where $\rho$, $\mathbf{u}$, $p$ and $s$ stand for the mixture density, velocity vector, static pressure and entropy per mass unit respectively while $r = C_p - C_v$ and $q$ is the rate of heat release per unit of volume. At last, $D/Dt = \partial/\partial t + \mathbf{u}\cdot\nabla$ is the material derivative. Together with the state equation and entropy expression

$$\frac{p}{\rho} = rT \qquad \text{and} \qquad s - s_{\rm st} = \int_{T_{\rm st}}^{T} \frac{C_p(T')}{T'}dT' - r\ln\left(\frac{p}{p_{\rm st}}\right), \tag{2.4}$$

where the 'st' index stands for standard values and $T$ is the static temperature, these transport equations describe the spatio-temporal evolutions of all relevant physical flow quantities.

The Linearized Euler Equations can be derived from Eq. 2.1 to 2.4 by considering the simple case of small amplitude fluctuations (index 1) super-imposed to a mean flow (index 0) which depends only on space. The instantaneous pressure, density, temperature, entropy and velocity fields can then be written as $p = p_0 + p_1$, $\rho = \rho_0 + \rho_1$, $T = T_0 + T_1$, $s = s_0 + s_1$ and $\mathbf{u} = \mathbf{u_0} + \mathbf{u_1}$ where the quantities $p_1/p_0$, $\rho_1/\rho_0$, $T_1/T_0$, $s_1/s_0$ and $\sqrt{\mathbf{u_1} \cdot \mathbf{u_1}}/c_0$ are of order $\epsilon$, where $\epsilon \ll 1$ and $c_0 = \sqrt{\gamma p_0/\rho_0}$ is the mean speed of sound. Injecting the above expansions for the instantaneous flow quantities into Eqs 2.1 to 2.4 and keeping only terms of order $\epsilon$, one obtains the following set of linear equations for the fluctuating quantities $\rho_1$, $\mathbf{u_1}$, $s_1$ and $p_1$:

$$\frac{\partial \rho_1}{\partial t} + \mathbf{u_1} \cdot \nabla \rho_\mathbf{0} + \rho_\mathbf{0} \nabla \cdot \mathbf{u_1} + \mathbf{u_0} \cdot \nabla \rho_\mathbf{1} + \rho_\mathbf{1} \nabla \cdot \mathbf{u_0} = \mathbf{0}, \tag{2.5}$$

$$\rho_0 \frac{\partial \mathbf{u}_1}{\partial t} + \nabla p_1 + \rho_0 \mathbf{u}_1 \cdot \nabla \mathbf{u}_0 + \rho_0 \mathbf{u}_0 \cdot \nabla \mathbf{u}_1 + \rho_1 \mathbf{u}_0 \cdot \nabla \mathbf{u}_0 = 0, \tag{2.6}$$

$$\frac{\partial s_1}{\partial t} + \mathbf{u}_1 \cdot \nabla s_0 + \mathbf{u}_0 \cdot \nabla s_1 = \frac{r q_1}{p_0} - \frac{r q_0}{p_0^2} p_1 \tag{2.7}$$

The linearized state equation and entropy expression are:

$$\frac{p_1}{p_0} - \frac{\rho_1}{\rho_0} - \frac{T_1}{T_0} = 0 \qquad \text{and} \qquad \frac{s_1}{C_v} = \frac{p_1}{p_0} - \gamma \frac{\rho_1}{\rho_0}. \tag{2.8}$$

### 2.2. *Linearized Euler Equations in frequency space*

Writing any fluctuating quantity $g_1(\mathbf{x}, t)$ as $g_1 = \hat{g}(\mathbf{x}) e^{-j\omega t}$, one obtains:

$$\hat{\mathbf{u}} \cdot \nabla \rho_0 + \rho_0 \nabla \cdot \hat{\mathbf{u}} + \mathbf{u_0} \cdot \nabla \hat{\rho} + \hat{\rho} \nabla \cdot \mathbf{u_0} = \mathbf{j} \omega \hat{\rho}, \tag{2.9}$$

$$\frac{1}{\rho_0} \nabla \hat{p} + \hat{\mathbf{u}} \cdot \nabla \mathbf{u}_0 + \mathbf{u}_0 \cdot \nabla \hat{\mathbf{u}} + \frac{\mathbf{u}_0 \cdot \nabla \mathbf{u}_0}{\rho_0} \hat{\rho} = j\omega \hat{\mathbf{u}}, \tag{2.10}$$

$$\hat{\mathbf{u}} \cdot \nabla s_0 + \mathbf{u}_0 \cdot \nabla \hat{s} + \frac{r q_0}{p_0^2} \hat{p} - \frac{r}{p_0} \hat{q} = j\omega \hat{s} \tag{2.11}$$

and

$$\frac{\hat{p}}{p_0} - \frac{\hat{\rho}}{\rho_0} - \frac{\hat{T}}{T_0} = 0 \qquad \text{and} \qquad \frac{\hat{s}}{C_v} = \frac{\hat{p}}{p_0} - \gamma \frac{\hat{\rho}}{\rho_0}. \tag{2.12}$$

Using Eq. 2.12 to eliminate $\hat{p}$ in equations 2.9, 2.10 and 2.11, one obtains:

$$\left(\nabla \cdot \mathbf{u_0} + \mathbf{u_0} \cdot \nabla\right) \hat{\rho} + \left(\nabla \rho_0 + \rho_0 \nabla\right) \cdot \hat{\mathbf{u}} = j\omega \hat{\rho}, \tag{2.13}$$

$$\left(\frac{\nabla c_0^2}{\rho_0} + \frac{\mathbf{u}_0 \cdot \nabla \mathbf{u}_0}{\rho_0} + \frac{c_0^2}{\rho_0} \nabla\right) \hat{\rho} + \left(\nabla \mathbf{u}_0 \cdot + \mathbf{u}_0 \cdot \nabla\right) \hat{\mathbf{u}} + (\gamma - 1) T_0 \left(\frac{\nabla p_0}{p_0} + \nabla\right) \hat{s} = j\omega \hat{\mathbf{u}}, \tag{2.14}$$

$$\frac{\gamma r q_0}{\rho_0 p_0} \hat{\rho} + \nabla s_0 \cdot \hat{\mathbf{u}} + \left(\mathbf{u}_0 \cdot \nabla + (\gamma - 1) \frac{q_0}{p_0}\right) \hat{s} - \frac{r}{p_0} \hat{q} = j\omega \hat{s} \tag{2.15}$$

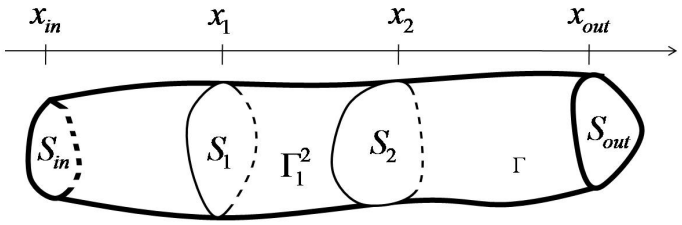


FIGURE 1. Definition of the flow domain for the derivation of the quasi-1D approximation.

Assuming that the unsteady heat release amplitude $\hat{q}$ is modeled as a linear operator of the amplitudes $\hat{\rho}$, $\hat{\mathbf{u}}$ and $\hat{s}$, formally written as $\hat{q} = q_{\hat{\rho}}\hat{\rho} + q_{\hat{\mathbf{u}}} \cdot \hat{\mathbf{u}} + q_{\hat{s}}\hat{s}$, equations 2.13, 2.14 and 2.15 define the following eigenvalue problem:

$$\mathcal{A}\mathcal{V} = j\omega\mathcal{V} \tag{2.16}$$

with

$$\mathcal{A} = \begin{bmatrix} \nabla \cdot \mathbf{u_0} + \mathbf{u_0} \cdot \nabla & \nabla\rho_0 \cdot + \rho_0\nabla\cdot & 0 \\ \frac{\nabla c_0^2}{\rho_0} + \frac{\mathbf{u}_0 \cdot \nabla \mathbf{u}_0}{\rho_0} + \frac{c_0^2}{\rho_0}\nabla & \nabla\mathbf{u}_0 \cdot + \mathbf{u}_0 \cdot \nabla & (\gamma-1)T_0\left(\frac{\nabla p_0}{p_0} + \nabla\right) \\ \frac{\gamma r q_0}{\rho_0 p_0} - \frac{r}{p_0}q_{\hat{\rho}} & \nabla s_0 \cdot - \frac{r}{p_0}q_{\hat{\mathbf{u}}}\cdot & \mathbf{u}_0 \cdot \nabla + (\gamma-1)\frac{q_0}{p_0} - \frac{r}{p_0}q_{\hat{s}} \end{bmatrix} \tag{2.17}$$

and $(\omega, \mathcal{V})$ the eigenpair, the eigenvector being $\mathcal{V} = (\hat{\rho}, \hat{\mathbf{u}}, \hat{s})^T$.

### 2.3. *Quasi-1D approximations*

In this paper, we restrict ourselves to 1D or quasi-1D configurations in order to focus on the mean Mach number effect, avoiding issues related to waves scattering by shear layers/vortices, complex geometries, and/or high order boundary conditions which are required when non planar, high frequency perturbations interact with the edge of the domain. Note that to remain consistent with the (quasi-)1D assumption that will be made hereafter, modes with 2D or 3D spatial structure must be excluded from the beginning. To this end, only frequencies smaller than the cut-off frequency of the duct will be considered in section 4. Another consequence of the quasi-1D framework is that vorticity perturbations are not present in the test cases considered, thus zeroing the acoustic/vorticity mode interactions which arise, even in the linear regime, as soon as the mean flow is non-uniform. However, since **a)** acoustic/entropy waves interactions can properly be accounted for under the 1D assumption and **b)** the entropy mode contains the largest part of the energy of the fluctuations when combustion is present [42], it is believed that 1D or quasi-1D configurations are relevant enough for studying the major effects of the baseline flow being not at rest.

The derivation of the quasi-1D counterparts of the equations of motion is rather standard; it is given in appendix for completeness and also because it is most often offered under the isentropic assumption. These equations describe the space-time evolution of small amplitude perturbations (subscript '1') super imposed to a steady baseline flow (subscript '0') defined over a quasi-1D flow domain $\Omega$ whose cross section area $\mathcal{S}$ is a slowly varying function of the principal axis of the domain, the $x$-direction say (see Fig. 1). After some algebra (see appendix), the following set of linear differential equations can be obtained for the cross section averaged fluctuating quantities:

$$\frac{\partial \rho_1}{\partial t} + u_1\frac{\partial \rho_0}{\partial x} + \rho_0\frac{\partial u_1}{\partial x} + u_0\frac{\partial \rho_1}{\partial x} + \rho_1\frac{\partial u_0}{\partial x} + \frac{\rho_0 u_1 + \rho_1 u_0}{\mathcal{S}}\frac{\partial \mathcal{S}}{\partial x} = 0, \tag{2.18}$$

$$\rho_0 \frac{\partial u_1}{\partial t} + \frac{\partial p_1}{\partial x} + \rho_0 u_1 \frac{\partial u_0}{\partial x} + \rho_0 u_0 \frac{\partial u_1}{\partial x} + \rho_1 u_0 \frac{\partial u_0}{\partial x} = 0, \tag{2.19}$$

$$\frac{\partial s_1}{\partial t} + u_1 \frac{\partial s_0}{\partial x} + u_0 \frac{\partial s_1}{\partial x} = \frac{r q_1}{p_0} - \frac{r q_0}{p_0^2} p_1 \tag{2.20}$$

Once written in the Fourier space, Eqs. 2.18-2.20 lead to an eigenvalue problem of the type Eq. 2.16 with the following quasi-1D linear operator in place of $\mathcal{A}$:

$$\mathcal{A}_{1\mathrm{D}} = \begin{bmatrix} \frac{\partial u_0}{\partial x} + u_0 \frac{\partial}{\partial x} + \frac{u_0}{\mathcal{S}} \frac{\partial \mathcal{S}}{\partial x} & \frac{\partial \rho_0}{\partial x} + \rho_0 \frac{\partial}{\partial x} + \frac{\rho_0}{\mathcal{S}} \frac{\partial \mathcal{S}}{\partial x} & 0 \\ \frac{1}{\rho_0} \frac{\partial c_0^2}{\partial x} + \frac{u_0}{\rho_0} \frac{\partial u_0}{\partial x} + \frac{c_0^2}{\rho_0} \frac{\partial}{\partial x} & \frac{\partial u_0}{\partial x} + \mathbf{u}_0 \frac{\partial}{\partial x} & (\gamma - 1) T_0 \left( \frac{1}{p_0} \frac{\partial p_0}{\partial x} + \frac{\partial}{\partial x} \right) \\ \frac{\gamma r q_0}{\rho_0 p_0} - \frac{r}{p_0} q_{\hat{\rho}} & \frac{\partial s_0}{\partial x} - \frac{r}{p_0} q_{\hat{u}} & u_0 \frac{\partial}{\partial x} + (\gamma - 1) \frac{q_0}{p_0} - \frac{r}{p_0} q_{\hat{s}} \end{bmatrix} \tag{2.21}$$

The eigenvector is now the 1D counterpart of $\mathcal{V}$, viz. $\mathcal{V}_{1\mathrm{D}} = (\hat{\rho}, \hat{u}, \hat{s})^T$.

The quasi-1D approximation is often used to described isentropic nozzles where the fluctuating motion remains isentropic if no entropy fluctuations are injected through the inlet $\mathcal{S}_{\mathrm{in}}$. In this case, the relevant equation has the form of Eq. 2.16 written for the following simplified quasi-1D acoustic operator in place of $\mathcal{A}$:

$$\mathcal{A}_{1\mathrm{D,ac}} = \begin{bmatrix} \frac{\partial u_0}{\partial x} + u_0 \frac{\partial}{\partial x} + \frac{u_0}{\mathcal{S}} \frac{\partial \mathcal{S}}{\partial x} & \frac{\partial \rho_0}{\partial x} + \rho_0 \frac{\partial}{\partial x} + \frac{\rho_0}{\mathcal{S}} \frac{\partial \mathcal{S}}{\partial x} \\ \frac{1}{\rho_0} \frac{\partial c_0^2}{\partial x} + \frac{u_0}{\rho_0} \frac{\partial u_0}{\partial x} + \frac{c_0^2}{\rho_0} \frac{\partial}{\partial x} & \frac{\partial u_0}{\partial x} + \mathbf{u}_0 \frac{\partial}{\partial x} \end{bmatrix} \tag{2.22}$$

The eigenvector is now the acoustic 1D counterpart of $\mathcal{V}_{1\mathrm{D}}$, viz. $\mathcal{V}_{1\mathrm{D,ac}} = (\hat{\rho}, \hat{u})^T$.

### 2.4. *1D Uniform ducts*

In general, there is no analytical solution to the set of equations 2.18-2.20, even in the 1D case where $\mathcal{S}$ is constant. However, it is sometimes possible to recast the mathematical problem into a single ordinary differential equation for a proper acoustic variable so that an analytical solution can be found [43–45]. One of the most general cases treated in this way corresponds to a 1D duct with linear temperature profile, constant pressure and velocity [46]; it is then possible, at least in the low Mach number regime, to derive a solvable hypergeometric equation for a mapping of the acoustic pressure. The easiest situation corresponds to an isothermal, isobaric zero Mach number mean flow where the above set of equations reduces to a second order, constant coefficient wave equation for the pressure fluctuations. It is then common use to seek for the harmonic solution of the form:

$$p_1(x,t) = Re\left[\hat{p}(x) exp\left(-j\omega t\right)\right], \qquad \text{with} \qquad \hat{p}(x) = \mathcal{A}^+ exp\left(jkx\right) + \mathcal{A}^- exp\left(-jkx\right)$$

where $\mathcal{A}^+ exp\left(jkx\right)$ and $\mathcal{A}^- exp\left(-jkx\right)$ stand for the forward and backward propagating waves respectively ($\mathcal{A}^+$ and $\mathcal{A}^-$ are the associated pre-exponential factors) and $k = \omega/c_0$ is the acoustic wave number. When the mean flow is not at rest but at constant speed $u_0$, the two waves do not propagate at the same speed and one uses instead:

$$\hat{p}(x) = \mathcal{A}^+ exp\left(jk^+ x\right) + \mathcal{A}^- exp\left(-jk^- x\right) \tag{2.23}$$

where $k^+ = \omega/(c_0 + u_0) = k/(1+M)$ and $k^- = \omega/(c_0 - u_0) = k/(1-M)$. Injecting this expression into Eq. 2.19 written under the uniform mean velocity assumption, one obtains:

$$\frac{d\hat{u}}{dx} - j\frac{k}{M}\hat{u} = -\frac{1}{\rho_0 u_0}\frac{d\hat{p}}{dx}, \tag{2.24}$$

so that the velocity complex amplitude reads:

$$\hat{u}(x) = \frac{1}{\rho_0 c_0}\left[\mathcal{A}^+ exp\left(jk^+ x\right) - \mathcal{A}^- exp\left(-jk^- x\right)\right] \tag{2.25}$$

Moreover, since the entropy perturbations propagate at the fluid velocity, one may write the corresponding complex amplitude as:

$$\hat{s}(x) = \mathcal{E} exp\,(jk_s x) \tag{2.26}$$

where $k_s = k/M$ is the entropy wave number. Injecting the above expressions of the complex amplitudes into Eqs. 2.12 one deduces:

$$\hat{\rho} = \frac{\hat{p}}{c_0^2} - \frac{\rho_0 \mathcal{E}}{C_p} e^{jk_s x} \qquad \text{and} \qquad \frac{\hat{T}}{T_0} = \frac{\gamma - 1}{\rho_0 c_0^2}\hat{p} + \frac{\mathcal{E}}{C_p} e^{jk_s x} \tag{2.27}$$

It follows from the above statements that describing the harmonic small amplitude perturbations over an isothermal, constant velocity 1D mean flow requires the calculation of three pre-exponential factors $\mathcal{A}^+$, $\mathcal{A}^-$ and $\mathcal{E}$. These complex valued coefficients are obtained by prescribing physical boundary conditions: when the mean flow is subsonic, two conditions must be given at the inlet section (as two waves enter the domain) and one at the outlet where only the backward propagating acoustic wave enters the domain. More interesting configurations can be considered by connecting $N$ uniform homentropic segments. This is what is done in the Low-order methods discussed in the introduction. At each interface, three jump relations are specified so that the $3N$ unknown waves (3 per segments) can be obtained thanks to the three inlet/outlet conditions and the $3(N-1)$ interface conditions. Assuming that such an interface is located at $x = x_i$, the jump conditions are obtained by integrating Eqs. A 8-A 10 between $x_i - \eta$ and $x_i + \eta$ and taking the limit $\eta \to 0^+$. In the case where the two connected ducts share the same cross section area $\mathcal{S}$, this leads to:

$$[\overline{\rho}\ \overline{u}] = 0, \tag{2.28}$$

$$[\overline{p} + \overline{\rho}\ \overline{u}\ \overline{u}] = 0, \tag{2.29}$$

$$[\overline{\rho}\ \overline{u}\ \overline{s}] = Q_s, \tag{2.30}$$

where $[\,]$ is the jump operator at interface $x = x_i$ and $Q_s$ is the volume integral of the RHS of Eq. A 10, viz. $q/T$. In this approach, the heat release $q$ is present only at the interface since each segment is homentropic; thus $q(x,t) = Q(t)\delta(x - x_i)$, where $\delta(x - x_i)$ is the Dirac distribution located at $x = x_i$. This interface heat release generates a temperature jump so that $Q_s$ cannot be interpreted easily. It is more suitable to use the total energy conservation equation in order to derive the third jump condition, viz.:

$$\frac{\partial \overline{\rho E}}{\partial t} + \frac{\partial \overline{\rho u H}}{\partial x} = \overline{q},$$

where the total energy is $E = C_v T + u^2/2$ and the total enthalpy reads $H = E + p/\rho = C_p T + u^2/2$. After integration between $x - \epsilon$ and $x + \epsilon$ one obtains:

$$\left[\overline{\rho}\ \overline{u}\ \overline{H}\right] = Q, \tag{2.31}$$

where the RHS is simply the total heat release. In terms of complex valued amplitudes of the fluctuations, one obtains the following jump relations by linearizing Eqs. 2.28, 2.29 and 2.31:

$$[\rho_0 \hat{u} + u_0 \hat{\rho}] = 0, \tag{2.32}$$

$$\left[\hat{p} + 2\rho_0 u_0 \hat{u} + u_0^2 \hat{\rho}\right] = 0, \tag{2.33}$$

$$\left[\left(C_p T_0 + \frac{1}{2}u_0^2\right)\ (\rho_0 \hat{u} + u_0 \hat{\rho}) + \rho_0 u_0 \left(C_p \hat{T} + u_0 \hat{u}\right)\right] = \hat{Q}, \tag{2.34}$$

where $Q(t) = Re\left(\hat{Q}exp(-j\omega t)\right)$.

### 2.5. *Zero Mach number mean flow*

When dealing with thermo-acoustic instabilities, it is often claimed that the mean Mach number is small enough to consider that the baseline flow is at rest. According to the order of magnitude analysis proposed by Nicoud et al. [29], 'small enough' means $M << \delta_f/L_a$, where $\delta_f$ and $L_a$ are the characteristic flame thickness and acoustic wavelength. Assuming $\mathbf{u_0} = \mathbf{0}$, taking the time derivative of Eq. 2.5, adding the divergence of Eq. 2.6 divided by $\rho_0$ and using Eqs. 2.8 and 2.7 to eliminate $\rho_1$ yield the following wave equation for the pressure fluctuations $p_1$:

$$\nabla \cdot \left(\frac{1}{\rho_0}\nabla p_1\right) - \frac{1}{\gamma p_0}\frac{\partial^2 p_1}{\partial t^2} = -\frac{\gamma - 1}{\gamma p_0}\frac{\partial q_1}{\partial t}. \tag{2.35}$$

Note that no assumption has been made about the spatial evolution of the isentropic coefficient $\gamma$ to derive Eq. 2.35. If $\gamma$ is constant over space, one recovers the classical equation for inhomogeneous medium with the elliptic term being $\nabla \cdot \left(c_0^2 \nabla p_1\right)$. Written in the frequency space, Eq. 2.35 leads to the classical Helmholtz equation :

$$\nabla \cdot \left(\frac{1}{\rho_0}\nabla \hat{p}\right) + \frac{\omega^2}{\gamma p_0}\hat{p} = i\omega\frac{\gamma - 1}{\gamma p_0}\hat{q}(\mathbf{x}), \tag{2.36}$$

Three types of boundary conditions are usually associated to Eq. 2.36 ($\mathbf{n}_{\mathrm{BC}}$ denotes the outward unit normal vector to the boundary $\partial\Omega$ of the flow domain):

- Zero pressure: this corresponds to fully reflecting outlets where the outer pressure is imposed strongly to the flow domain, zeroing the pressure fluctuations:

$$\hat{p} = 0, \qquad \text{on the boundary } \partial\Omega_D, \tag{2.37}$$

- Zero normal velocity, viz. $\hat{u} \cdot \mathbf{n}_{\mathrm{BC}} = 0$: this corresponds to fully rigid walls or reflecting inlets where the velocity of the incoming flow is imposed, zeroing the velocity fluctuations. Under the zero Mach number assumption, Eq. 2.6 can be used to re-write this condition as a Neumann condition for the acoustic pressure:

$$\nabla \hat{p} \cdot \mathbf{n}_{\mathrm{BC}} = 0, \qquad \text{on the boundary } \partial\Omega_N, \tag{2.38}$$

- Imposed reduced complex impedance $Z = \hat{p}/\rho_0 c_0 \hat{\mathbf{u}} \cdot \mathbf{n}_{\mathrm{BC}}$. Under the zero Mach number assumption, this condition can be re-written as a Robin condition for the acoustic pressure:

$$c_0 Z \nabla \hat{p} \cdot \mathbf{n}_{\mathrm{BC}} - i\omega\hat{p} = 0, \qquad \text{on the boundary } \partial\Omega_Z, \tag{2.39}$$

Associated with the homogeneous boundary conditions 2.37, 2.38 and 2.39 on $\partial\Omega = \partial\Omega_D \bigcup \partial\Omega_N \bigcup \partial\Omega_Z$, equation 2.36 defines a non-linear eigenvalue problem which can be solved as soon as a model is provided for the unsteady heat release $\hat{q}$.

### 2.6. *Flame model*

Modeling the unsteady behavior of the flame is the most challenging part in the description of thermo-acoustic instabilities [47]. Several models have been proposed in the past to describe the response of conic or V-shape laminar flames [48], accounting for non-linear saturation effects [49] and equivalence ratio fluctuations [50, 51]. Most models available so far relate the global heat release across the flame zone to the acoustic velocity in the cold gas region upstream the flame. For example the $n - \tau$ model [52, 53] reads:

$$\hat{Q} = \mathcal{S}_{\mathrm{ref}}\frac{\gamma p_0}{\gamma - 1}\; n\; \exp(i\omega\tau)\hat{u}(x_f^-), \tag{2.40}$$

where $n$ and $\tau$ denote the interaction index and time delay, $\hat{Q}$ is the complex valued amplitude of the total unsteady heat release over the flow domain, viz. $\int_x \hat{q}(x)dx$ and $\mathcal{S}_{\rm ref}$ is the cross section area of the duct. At last, $\hat{u}(x_f^-)$ is the velocity perturbation immediately upstream of the flame interface. This modeling strategy is supported by the idea that heat release depends on the flame surface which, the flame speed being given, is mainly controlled by a time lagged version of the fresh gas flow rate. As an extension to the *global* $n-\tau$ model, Eq. 2.40, it is rather natural to relate the pointwise unsteady heat release $\hat{q}(\mathbf{x})$ to an upstream reference acoustic velocity through a *local* $n-\tau$ model [29]. This amounts to:

$$\frac{q_1(\mathbf{x},t)}{q_{\rm tot}} = n_{\mathbf{u}}(\mathbf{x}) \frac{\mathbf{u}_1(\mathbf{x}_{\rm ref}, t-\tau_{\mathbf{u}}(\mathbf{x}))\cdot \mathbf{n}_{\rm ref}}{U_{\rm bulk}}, \tag{2.41}$$

where $n_{\mathbf{u}}(\mathbf{x})$ and $\tau_{\mathbf{u}}(\mathbf{x})$ are fields of interaction index and time lag and $\mathbf{n}_{\rm ref}$ is a fixed unitary vector defining the direction of the reference velocity. The scaling by the total heat release $q_{\rm tot}$ and the bulk velocity $U_{\rm bulk}$ has been used to make sure that $n_{\mathbf{u}}(\mathbf{x})$ has no dimension. Once converted into the frequency space, this model leads to

$$\hat{q}(\mathbf{x}) = \frac{q_{\rm tot}}{U_{\rm bulk}} n_{\mathbf{u}}(\mathbf{x}) e^{j\omega\tau_{\mathbf{u}}(\mathbf{x})} \hat{\mathbf{u}}(\mathbf{x}_{\rm ref})\cdot\mathbf{n}_{\rm ref}. \tag{2.42}$$

where the acoustic velocity can be replaced by the pressure gradient ($j\omega\hat{u} = \nabla\hat{p}/\rho_0$) if the zero Mach number assumption is made.

## 3. CONFIGURATIONS AND NUMERICAL TOOLS

Three different numerical tools have been used in the course of this study to solve the different mathematical formulations discussed in section 2, all of them being based on the linear assumption:

- The general purpose AVSP code [29] for the computation of the thermo-acoustic modes in complex geometries from the resolution of Eq. 2.36, viz. assuming zero Mach number mean flow,
- The tool NOZZLE for the computation of the acoustic impedance of accelerated regions from the resolution of equations related to the quasi-1D acoustic operator of Eq. 2.22. NOZZLE aims at producing relevant boundary conditions for thermo-acoustic analysis based on Eq. 2.36 and for which the accelerated regions must be excluded from the computational domain,
- The tool LEE-Q1D for computing the modes related to the quasi 1D Linearized Euler Equations from the eigenvalue problem defined by Eqs. 2.16 and 2.21.

These three numerical tools are described in the following sections.

### 3.1. *Thermo-acoustic modes with zero Mach number - The AVSP code*

Assuming that the sound speed $c_0$ and the density $\rho_0$ distributions over space are known, Eq. 2.36 can be solved for the pressure amplitude and the frequency as soon as a model provides the unsteady heat release $\hat{q}$ from the knowledge of the acoustic field $\hat{p}$. A Galerkin finite element method can be used to transform Eq. 2.36 into a nonlinear eigenvalue problem of size close to N (the number of nodes in the finite element grid used to discretize the geometry) of the form:

$$[A][P] + \omega[B(\omega)][P] + \omega^2[C][P] = [D(\omega)][P] \tag{3.1}$$

where $[P]$ is the column vector containing the nodal values of the eigenmode at frequency $\omega$ and $[A]$ and $[C]$ are square matrices depending only on the discretized geometry of the

combustor and mean flow fields $c_0$ and $\rho_0$. Matrix $[B]$ contains information related to the boundary conditions and thus depends on $\omega$ since in general $Z$ is frequency dependent. Matrix $[D]$ contains the unsteady contribution of the flame, viz. $\hat{q}$, and usually depends non-linearly on the mode frequency $\omega$ (see Eq. 2.42). Thus, Eq. 3.1 defines a non-linear eigenvalue problem which must be solved iteratively, the $k^{th}$ iteration consisting in solving the quadratic eigenvalue problem in $\omega_k$ defined as:

$$([A] - [D(\omega_{k-1})])\,[P] + \omega_k[B(\omega_{k-1})][P] + \omega_k^2[C][P] = 0. \tag{3.2}$$

A natural initialization is to set $[D](\omega_0) = 0$ so that the computation of the modes without acoustic/flame coupling is in fact the first step of the iteration loop. Usually, only a few (typically less than 5) iterations are enough to converge toward the complex frequency and associated mode.

Note that a quadratic problem must be solved at each iteration Eq. 3.2. These problems are rather well known from a theoretical point of view; they can efficiently be solved numerically once converted into an equivalent linear problem of size $2\times N$ [54]; we are then using a parallel implementation of the Arnoldi method [55] available in the P-ARPACK library. Another option is to solve the quadratic eigenvalue problem directly without linearizing it; a specific algorithm must then be used instead of the Arnoldi approach. A good candidate is the Jacobi-Davidson method [56] which has recently been applied successfully to combustion instability problems [57]. However, since computational time is not an issue in the present study (only simple geometries are considered), the well established Arnoldi method has been used. More details regarding the AVSP code can be found in [29].

### 3.2. *Acoustic impedance of non-compact nozzles - The NOZZLE code*

The purpose of the NOZZLE tool is to compute the acoustic impedance of diffusers/nozzles under the isentropic mean flow assumption; it can be seen as a way to extend previous analytical results [38] to non compact nozzles. The appropriate equations to be considered are the quasi-1D linearized Euler equations written in the frequency space and under the constant mean entropy assumption. These equations can thus be written under the form:

$$\mathcal{A}_{\mathrm{1D,ac}}\mathcal{V}_{\mathrm{1D,ac}} - j\omega\mathcal{V}_{\mathrm{1D,ac}} = 0 \tag{3.3}$$

with $\mathcal{V}_{\mathrm{1D,ac}} = (\hat{\rho}, \hat{u})^T$ and $\mathcal{A}_{\mathrm{1D,ac}}$ given as in Eq. 2.22. Although formally similar to Eq. 2.16, the above equation should not be interpreted as an eigenvalue problem but rather as a linear system of equations whose unknown is $\mathcal{V}_{\mathrm{1D,ac}}$, assuming that the frequency $\omega$ is fixed a priori. Once discretized, Eq. 3.3 can be converted into an algebraic linear system of size close to twice the number of grid points:

$$[A_{\mathrm{1D,ac}}][V_{\mathrm{1D,ac}}] = [BT] \tag{3.4}$$

where $V_{\mathrm{1D,ac}}$ is the discrete counterpart of the vector of acoustic unknowns $\mathcal{V}_{\mathrm{1D,ac}}$, the matrix $[A]$ depends on both $\omega$ and the details of the spatial discretization and the right-hand-side term comes from possibly non homogeneous boundary conditions. In the present study, a first order upwind biased finite difference approximation has been used to discretize Eq. 3.3.

For any quasi-1D flow domain with inlet and outlet section $\mathcal{S}_{\mathrm{in}}$ and $\mathcal{S}_{\mathrm{out}}$ respectively (see figure 1), the following procedure is used to compute the equivalent acoustic impedance:

($a$) fix the frequency $\omega$,

($b$) impose a non zero forward propagating acoustic wave at the inlet section $\mathcal{S}_{\rm in}$. The corresponding boundary condition is obtained by combining Eqs. 2.23 and 2.25 to relate $\hat{p}$ and $\hat{u}$ at $x = x_{\rm in}$, viz.

$$2\mathcal{A}^+ exp\left(jk^+ x_{\rm in}\right) = \hat{p} + \rho_0 c_0 \hat{u},$$

where $\mathcal{A}^+$ is set to any non zero value to ensure that the inlet condition is non homogeneous,

($c$) define the appropriate boundary condition to be prescribed at the outlet section depending on whether the mean flow is subsonic or supersonic, typically imposed pressure or no boundary condition respectively,

($d$) solve the corresponding linear system Eq. 3.4,

($e$) compute the acoustic equivalent impedance as $Z_{\rm in} = \hat{p}/\rho_0 c_0 \hat{u}$ assessed at $x = x_{\rm in}$.

Note that when the mean flow is subsonic, there is a backward propagating wave entering the domain through the outlet section $\mathcal{S}_{\rm out}$ so that an outlet boundary condition is required. In this case case, the above procedure turns out to provide a way to transform a supposedly known acoustic boundary condition at $\mathcal{S}_{\rm out}$ to another condition at $\mathcal{S}_{\rm in}$. For example, when the flow domain is a nozzle, this procedure allows to displace an acoustic boundary condition at a high speed section to an upstream, low Mach number position. In the case where the nozzle is choked, no extra acoustic condition is required since no wave can enter the domain through the outlet section $\mathcal{S}_{\rm out}$. In the particular case where the outlet section coincides with the location of the throat, the proper acoustic impedance to impose at $\mathcal{S}_{\rm out}$ is given by Lieuwen and Yang [5]:

$$Z_{\rm th} = \frac{2\frac{du_0}{dx} - j\omega}{(\gamma - 1)\frac{du_0}{dx} - j\omega} \tag{3.5}$$

and the procedure above allows to convert this impedance condition valid at the sonic throat to another condition valid at an upstream, low Mach number location.

### 3.3. *Thermo-acoustic modes with non-zero Mach number - The LEE-Q1D code*

The proper framework for this tool are the Linearized Euler Equations written in the frequency space under the quasi-1D approximation, Eq. 2.16, with the matrix operator defined as in Eq. 2.21, viz.

$$\mathcal{A}_{\rm 1D}\mathcal{V}_{\rm 1D} = j\omega\mathcal{V}_{\rm 1D} \tag{3.6}$$

Using an appropriate spatial discretization leads to an algebraic eigenvalue problem of the form:

$$[A_{\rm 1D}][V_{\rm 1D}] = j\omega[V_{\rm 1D}] \tag{3.7}$$

where obvious notations have been used. Note that similarly to the situation depicted in section 3.1, the $[A_{\rm 1D}]$ matrix may depend on the frequency $\omega$ as soon as frequency dependent boundary conditions are considered; in this case the above eigenvalue problem cannot be solved directly by the Arnoldi algorithm but requires an iterative procedure similar to Eq. 3.2.

Since the entropy fluctuations are kept in this formulation, viz. $\mathcal{V}_{\rm 1D} = (\hat{\rho}, \hat{u}, \hat{s})^T$, the size of matrix $[A_{\rm 1D}]$ is close to three times the number of grid points. In the course of this study, a mixed second order centered/first order upwind biased finite difference approximation has been used in order to generate the $[A_{\rm 1D}]$ matrix from the mathematical expression given in Eq. 2.21 (centered scheme for the $\hat{\rho}$ and $\hat{u}$ equations, upwind biased scheme for the $\hat{s}$ equation); a staggered grid arrangement (velocity stored at the cell edges, density and entropy fluctuations stored at the cell centers) has been used in order to avoid the pressure field to be contaminated by the classical odd-even decoupling phenomenon.

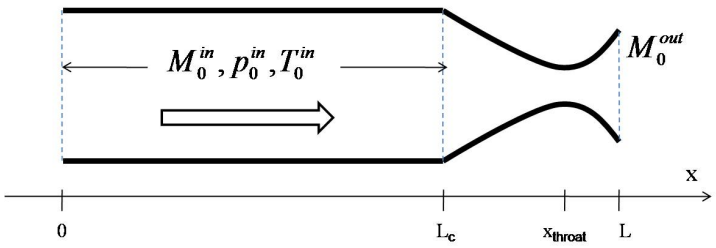


FIGURE 2. Principle of the academic configuration for studying the mean Mach number effects with respect to the boundary conditions (choked nozzle).

| $L$ (m) | $L_c$ (m) | $\gamma$ | $r$ (S.I) | $p_0$ (Pa) | $T_0$ (K) |
|---|---|---|---|---|---|
| 1.0 | 0.9 | 1.4 | 287 | 101325 | 300 (K) |

TABLE 1. Main physical parameters used for configuration of Fig. 2.

## 4. RESULTS

The tools described in section 3 are now used to perform the thermo-acoustic analysis of several academic configurations with the aim to assess the Mach number effects on the resulting modes of oscillation. All the results presented are essentially free of numerical errors since grid convergence has been obtained in all the cases discussed. Typically, 1000 to 3000 grid points were used to represent the quasi-1D configurations discussed in the following sections. The height of the ducts considered in the following sections are not specified since only 1D modes are considered; it may simply be though as small enough to ensure that the frequencies discussed are smaller than the cutoff frequency of the corresponding configuration.

### 4.1. *Baseline flow effect on the boundary conditions*

#### 4.1.1. *Academic configuration I*

The configuration considered in this section is shown in figure 2. It consists in a constant cross section channel (the combustion chamber) of length $L_c$ mounted on a nozzle (the high pressure distributor or first compressor stage) of length $L - L_c$. The mean flow is assumed isentropic so that it is uniform over the combustion chamber, with $M_0^{\text{in}}$ the corresponding Mach number. The nozzle profile has been designed from the classical isentropic mean flow equations so that it produces an increase in the mean Mach number of the form:

$$M(x) = M_0^{\text{in}} + \left(M_0^{\text{out}} - M_0^{\text{in}}\right) \left(\frac{x - L_c}{L - L_c}\right)^3, \tag{4.1}$$

for $x \geq L_c$. The nozzle can be made choked (resp. unchoked) by setting the exit Mach number $M_0^{\text{out}}$ larger (resp. smaller) than unity; the duct between $L_c$ and $L$ has a convergent-divergent shape if choked and is convergent otherwise. When a throat is present it is located at $x_{\text{throat}}$. The effect of upstream Mach number can be assessed by considering different inlet Mach number values. The geometrical, physical and inlet baseline flow parameters that have been used are given in table 1 from which one can deduce the following inlet speed of sound and density: $c_0 \simeq 347.2$ m/s and $\rho_0 \simeq 1.177$ kg/m$^3$.

The two main cases considered in the following correspond to $M_0^{\text{out}} = 0.8$ and $M_0^{\text{out}} = 1.5$ respectively, values chosen as representative to the distributor of a gas turbine under

idle and standard operating conditions respectively. In each case, different inlet Mach number values have been considered, viz. $M_0^{\text{in}} = 0.01$; 0.1; 0.2; 0.3 and 0.4 while zero velocity fluctuation is assumed at the inlet section ($\hat{u}(x=0)=0$). Note that the modal analysis can only be performed for homogeneous boundary conditions so that the algebraic problem which results from the spatial discretization is indeed an eigenvalue problem. To this respect, the most natural choice for the entropy fluctuations is to use a Dirichlet condition at the inlet, viz. $\hat{s}(x=0)=0$. In absence of a mean entropy gradient and combustion, the equation for the entropy fluctuations then reduces to (see Eq. 2.21):

$$u_0 \frac{d\hat{s}}{dx} = j\omega\hat{s}, \qquad \text{with} \quad \hat{s}(x=0)=0,$$

whose only solution is $\hat{s}=0$. The configuration depicted in Fig. 2 is thus purely acoustic and the modal analysis can be equivalently done with Eq. 2.21 or Eq. 2.22.

#### 4.1.2. *Modal analysis*

The modal analysis of the cases described above has been performed in two different ways in order to assess to error related to the zero Mach number assumption for the mean flow:

($a$) **Method M1**: by solving the eigenvalue problem associated to the quasi-1D Linearized Euler Equations discretized over the entire domain $0 \le x \le L$ (LEE-Q1D tool of section 3.3). Since no specific assumption is made regarding the nozzle compactness or the mean Mach number, this approach provides the reference solution. Note that it has been checked in the choked nozzle case, as expected from a theoretical point of view, that the results do not change if the computational domain is restricted to $0 \le x \le x_{\text{restrict}}$ where $x_{\text{restrict}}$ is anywhere between the throat location $x_{\text{throat}}$ and the original domain outlet $x=L$. In the unchoked nozzle case, a zero pressure fluctuation condition is imposed at the outlet section,

($b$) **Method M2**: by solving the eigenvalue problem associated to the Helmholtz equation derived under the zero Mach number assumption for the mean flow and discretized over the combustion chamber, viz. $0 \le x \le L_c$ (AVSP code of section 3.1). The outlet boundary condition is then obtained from the impedance assessed at $x=L_c$ from the technique described in section 3.2 (NOZZLE tool). Consistently with the previous item, the outlet pressure is zeroed at $x=L$ when computing the equivalent impedance of an unchocked nozzle while the condition Eq. 3.5 has been used at $x=x_{\text{throat}}$ in the choked case.

Note that the way to proceed depicted in item (b) is strictly equivalent to what is done in practical modal analysis of complex geometries [29, 31] so that the comparison proposed in the following provides a relevant assessment of the error related to the zero Mach number assumption for the mean flow with respect to the outlet condition.

#### 4.1.3. *Results*

The first eigen-frequencies obtained when applying methods **M1** and **M2** of section 4.1.2 to the academic configuration of section 4.1.1 are given in table 2, for both the unchoked and the choked cases. The frequency dependent boundary impedances used at $x=L_c$ for method **M2** are illustrated for the choked case in figure 3 which displays the modulus and argument of the reflexion coefficient $R=(Z-1)/(Z+1)$. For all the Mach number values considered, the argument of $R$ tends to zero for vanishing frequencies, in agreement with the real valued impedance found by Marble and Candel [38] under

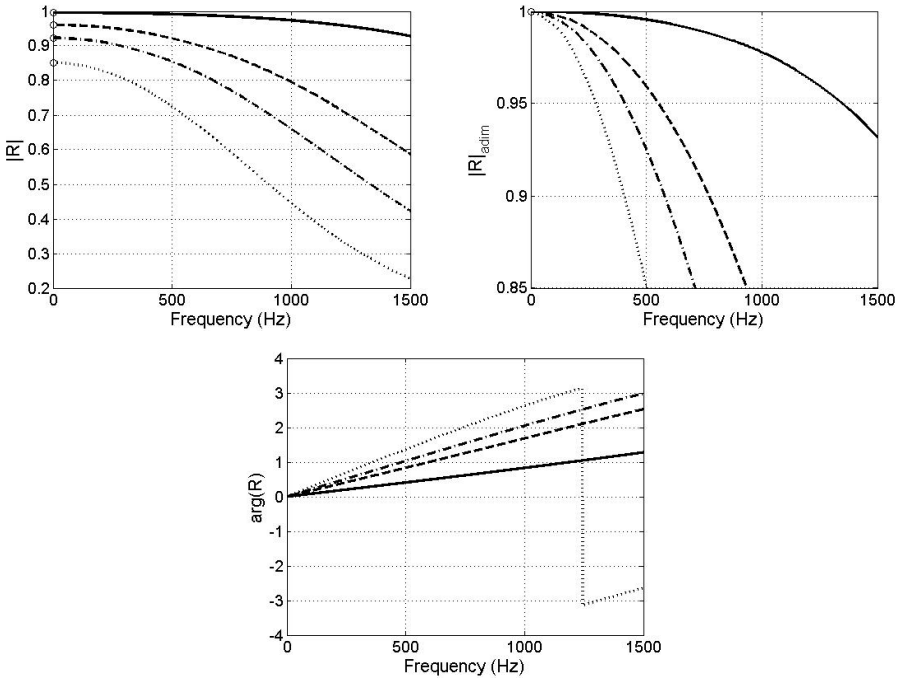


FIGURE 3. Outlet reflexion coefficient computed from NOZZLE (section 3.2) for the choked case: **Top left**: modulus; **Top right**: non-dimensionalized modulus; **Bottom**: phase. —— :$M_0^{\rm in} = 0.01$; – – – :$M_0^{\rm in} = 0.1$; —·— :$M_0^{\rm in} = 0.2$; ····· :$M_0^{\rm in} = 0.4$. Symbols denote the compact approximation $Z = 2/(\gamma-1)M_0^{\rm in}$.

the compact nozzle approximation, viz. $Z = 2/(\gamma-1)M_0^{\rm in}$, and corresponding reflexion coefficient $R = \big(1-(\gamma-1)M_0^{\rm in}/2\big) \,/\, \big(1+(\gamma-1)M_0^{\rm in}/2\big)$. Note that this approximation is in full agreement with the numerical assessments for small frequency values. Fig. 3 also indicates that the range of validity of the compact approximation is smaller for larger Mach numbers. For example, for $M_0^{\rm in} = 0.01$, the actual modulus of $R$ is 5 % off its compact approximation for $f \simeq 1300$ Hz, whereas the same error is obtained at $f \simeq 300$ Hz for $M_0^{\rm in} = 0.4$. This suggests that the critical Helmholtz number $f(L-L_c)/c_0$ below which the compact nozzle approximation is justified does in fact depend on the Mach number; it would be approx. 0.35 for $M_0^{\rm in} = 0.01$ but only 0.085 for $M_0^{\rm in} = 0.4$. The same trend can be observed for the phase of the reflexion coefficient.

In table 2, the relative error is defined as $2(\phi_{\rm M2}-\phi_{\rm M1})/(\phi_{\rm M2}-\phi_{\rm M1})$, where $\phi$ stands for either the real or imaginary part of the frequency and the index M1 (resp. M2) denotes Method **M1** (resp. Method **M2**). As expected, the error is essentially zero for the smallest inlet Mach number, $M_0^{\rm in} = 0.01$, since in this case the zero Mach number assumption for the mean flow is fully justified. For higher values of the Mach number within the combustion chamber, the **M2** method systematically overestimates the frequency amplitude (relative errors are always positive), significant errors (10 % or more) being obtained for inlet Mach numbers larger than 0.2. Note also that the error behaves essentially in the same way for both the unchoked and choked case, indicating that the main source of error is indeed the combustion chamber.

The relative error in the frequency of oscillation can actually be retrieved by the following simple reasoning. Calling $T^+$ and $T^-$ the times of propagation of an acoustic perturbation traveling throughout the combustion chamber in the forward and backward

| $M_0^{\text{in}}$ | Method **M1** | Method **M2** | $\epsilon_r$ | $\epsilon_i$ | $\epsilon_{\text{th}}$ |
|---|---|---|---|---|---|
| 0.01 | $187.23 - 0.48i$ | $187.24 - 0.49i$ | 0.0 | 2.1 | 0.0 |
| 0.10 | $180.57 - 4.61i$ | $182.45 - 4.87i$ | 1.0 | 5.5 | 1.0 |
| 0.20 | $173.53 - 9.15i$ | $180.96 - 10.08i$ | 4.2 | 9.7 | 4.1 |
| 0.30 | $163.75 - 13.93i$ | $180.33 - 16.30i$ | 9.6 | 15.7 | 9.4 |
| 0.40 | $151.25 - 19.54i$ | $180.68 - 24.64i$ | 17.7 | 23.3 | 17.4 |
| 0.01 | $188.19 - 0.14i$ | $188.22 - 0.12i$ | 0.0 | 15.4 | 0.0 |
| 0.10 | $181.62 - 1.31i$ | $183.54 - 1.40i$ | 1.1 | 6.6 | 1.0 |
| 0.20 | $173.90 - 2.48i$ | $181.42 - 2.77i$ | 4.2 | 11.0 | 4.1 |
| 0.30 | $163.11 - 3.45ii$ | $179.68 - 4.15i$ | 9.7 | 18.4 | 9.4 |
| 0.40 | $149.01 - 4.17i$ | $177.86 - 5.56i$ | 17.7 | 28.6 | 17.4 |

TABLE 2. First eigenfrequencies (Hz) obtained from Methods **M1** and **M2** for the unchoked ($M_0^{\text{out}} = 0.8$ - first five rows) and choked ($M_0^{\text{out}} = 1.5$ - last five rows) case. The forth and fifth columns contained the relative error (%) for the real and imaginary part of the frequencies respectively. The last column is $2(M_0^{\text{in}})^2/(2-(M_0^{\text{in}})^2)$.

| $M_0^{\text{in}}$ | 0.01 | 0.1 | 0.2 | 0.4 |
|---|---|---|---|---|
| Numerical impedance | $188.22 - 0.12i$ | $183.54 - 1.40i$ | $181.42 - 2.77i$ | $177.86 - 5.56i$ |
| Compact nozzle | $192.86 - 0.12i$ | $190.95 - 1.22i$ | $185.13 - 0.50i$ | $162.02 - 4.13i$ |

TABLE 3. First eigenfrequencies (Hz) obtained from Method **M2** for the choked nozzle case by using either the numerically (see section 3.2) or analytically (compact approximation - [38]) assessed outlet impedance at $x = L_c$.

direction respectively, viz. $T^+ = L_c/c_0(1+M_0^{\text{in}})$ and $T^- = L_c/c_0(1-M_0^{\text{in}})$, the frequency of oscillation can be assessed as $f \simeq 1/(T^+ + T^-) = c_0(1-(M_0^{\text{in}})^2)/2L_c$. Comparing the classical zero Mach number value of the frequency $f_0 = c_0/2L_c$ against $f$, the theoretical relative error is then $\epsilon_{\text{th}} = 2(f_0 - f)/(f_0 + f) \simeq 2(M_0^{\text{in}})^2/(2-(M_0^{\text{in}})^2)$. As shown in table 2, this assessment nicely reproduces the observed results.

The frequencies obtained numerically and reported in table 2 can be further validated since the problem actually considered when method **M2** is used can be solved semi-analytically. Indeed, since the combustion chamber is a constant cross section duct, Eqs. 2.23-2.25 are suitable to represent the acoustic fluctuations. The upstream boundary condition $\hat{u}(x = 0) = 0$ imposes the equality of the wave amplitudes, viz. $\mathcal{A}^+ = \mathcal{A}^-$, whereas the outlet impedance condition allows writing a dispersion relation of the form:

$$exp\left(jk^+L_c\right) + exp\left(-jk^-L_c\right) = Z(\omega)\left[exp\left(jk^+L_c\right) - exp\left(-jk^-L_c\right)\right] \qquad (4.2)$$

Assuming that $Z(\omega)$ is known (either analytically or numerically), Eq. 4.2 can be solved numerically to obtain the corresponding eigen-frequencies. If the boundary impedance depicted in Fig. 3 is injected into Eq. 4.2, the frequencies obtained are essentially the same as those given in the method **M2** column of table 2, supporting the fact that the results presented are essentially free of numerical errors. However, if the analytical approximation of Marble and Candel [38] is used instead, viz. $Z = 2/(\gamma - 1)M_0^{\text{in}}$, table 3 shows that some differences in the frequencies can be observed. These differences are moderate (less than 5 %), as it could have been anticipated from the previous discussion of Fig. 3 (the first eigenmode frequency is below 300 Hz). Note however that larger errors can be obtained for higher order modes (e.g. $486 - 0.5i$ instead of $454 - 0.5i$ for the third

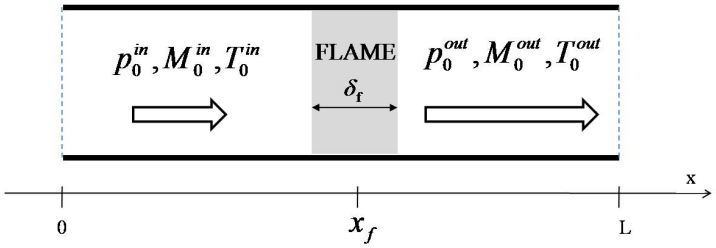


FIGURE 4. Principle of the academic configuration for studying the mean Mach number effects with respect to the flame/acoustic coupling.

mode at $M_0^{\text{in}} = 0.4$). Still, the main result from this isentropic configuration is that **a)** the errors from the zero Mach number assumption for the mean flow are moderate for moderate Mach numbers and **b)** that the main source of error is the change in the speed of propagation of the pressure waves rather that the boundary conditions themselves.

### 4.2. *Mean flow effect on the flame/acoustic coupling*

#### 4.2.1. *Academic configuration II*

The configuration considered in this section is shown in figure 4. It consists in a constant cross section channel of length $L$ with a 1D flame of characteristic thickness $\delta_f$ located at $x = x_f$. The mean flow is isentropic only in regions where combustion does not occur. Due to thermal expansion, the mean flow velocity increases continuously from $u_0^{\text{in}}$ to $u_0^{\text{out}}$ when the gas mixture is heated from $T_0^{\text{in}}$ to $T_0^{\text{out}}$. The baseline flow is defined in order to ensure constant mass flux $m_0 = \rho_0 u_0$, impulsion $J_0 = p_0 + \rho_0 u_0^2$ and conservation of the total temperature, viz. $\rho_0 u_0 C_p dT_{t0}/dx = q_0$, with $T_{t0} = T_0 + u_0^2/(2C_p)$. More precisely the following analytical evolution for static temperature has been selected in order to mimic the presence of an anisentropic region (the flame):

$$T_0 = \frac{T_0^{\text{in}} + T_0^{\text{out}}}{2} + \frac{T_0^{\text{out}} - T_0^{\text{in}}}{2} \tanh\left(3\,\frac{x - x_f}{\delta_f}\right), \tag{4.3}$$

The mean flow is then entirely determined by the choice of three independent quantities, for example the inlet pressure $p_0^{\text{in}}$, temperature $T_0^{\text{in}}$, Mach number $M_0^{\text{in}}$. Since the objective is to assess the mean flow effects related to the flame, simple acoustic boundary conditions are used in this section: zero velocity fluctuation at the inlet ($\hat{u}(x = 0) = 0$) and pressure fluctuation at the outlet ($\hat{p}(x = L) = 0$). As for the academic configuration I described in section 4.1.1, the most natural homogeneous boundary condition is $\hat{s}(x = 0) = 0$ so that only entropy fluctuations arising from the flame-acoustic coupling will be present in the modes computed.

#### 4.2.2. *Modal analysis*

The mean flow effects on the thermo-acoustic modes of configuration II are assessed by comparing the results using methods **M1** and **M2** (as defined in section 4.1.2) with various inlet Mach numbers. Note that the problem depicted in Fig. 4 can be solved semi-analytically in the limit case where $\delta_f \longrightarrow 0$ [33]. The mean flow is then isentropic in each of the two subdomains $0 \leq x < x_f$ and $x_f < x \leq L$ separated by the infinitely thin flame located at $x_f$. Thus harmonic pressure, velocity and entropy fluctuations are given as in Eqs. 2.23, 2.25 and 2.26 in each of the above domains and the solution is entirely known as soon as six wave amplitudes have been determined: two acoustic and one entropy wave in each sub-domain, viz. $\mathcal{A}_u^+$, $\mathcal{A}_u^-$, $\mathcal{E}_u$, $\mathcal{A}_b^+$, $\mathcal{A}_b^-$, and $\mathcal{E}_b$, with index 'u'

and 'b' denoting the unburnt and burnt gas respectively. From the boundary condition $\hat{s}(x=0)=0$, it follows immediately that $\mathcal{E}_u=0$ so that only five wave amplitudes need to be computed. These waves are solutions of an homogeneous linear system of equations obtained by requiring that the boundary conditions ($\hat{u}(x=0)=0$, $\hat{p}(x=L)=0$) and jump relations Eqs. 2.32-2.34 are fulfilled. After some algebra one obtains:

$$\mathcal{M}\mathcal{W}=0 \tag{4.4}$$

with

$$\mathcal{M}=\begin{bmatrix} (1+M_u)e^{jk_u^+x_f} & (M_u-1)e^{-jk_u^-x_f} & -(M_b+1)\frac{c_u}{c_b}e^{jk_b^+x_f} & -(M_b-1)\frac{c_u}{c_b}e^{-jk_b^-x_f} & M_b\frac{c_u}{c_b} \\ (1+M_u)^2e^{jk_u^+x_f} & (M_u-1)^2e^{-jk_u^-x_f} & -(M_b+1)^2e^{jk_b^+x_f} & -(M_b-1)^2e^{-jk_b^-x_f} & M_b^2 \\ \mathcal{M}_{31} & \mathcal{M}_{32} & \mathcal{M}_{33} & \mathcal{M}_{34} & M_b^3/2 \\ 1-Z_u & 1+Z_u & 0 & 0 & 0 \\ 0 & 0 & (1-Z_b)\ e^{jk_b^+L} & (1+Z_b)\ e^{-jk_b^-L} & 0 \end{bmatrix}, \tag{4.5}$$

$$\begin{aligned} \mathcal{M}_{31} &= \frac{c_u}{c_b}\left((1+M_u)\left[M_u+1/(\gamma-1)+M_u^2/2\right]+ne^{j\omega\tau}/(\gamma-1)\right)e^{jk_u^+x_f} \\ \mathcal{M}_{32} &= \frac{c_u}{c_b}\left((1-M_u)\left[M_u-1/(\gamma-1)-M_u^2/2\right]-ne^{j\omega\tau}/(\gamma-1)\right)e^{-jk_u^-x_f} \\ \mathcal{M}_{33} &= -(1+M_b)\left[M_b+1/(\gamma-1)+M_b^2/2\right]e^{jk_b^+x_f} \\ \mathcal{M}_{34} &= -(1-M_b)\left[M_b-1/(\gamma-1)-M_b^2/2\right]e^{-jk_b^-x_f}, \end{aligned} \tag{4.6}$$

and $\mathcal{W}=\left(\mathcal{A}_u^+\ \mathcal{A}_u^-\ \mathcal{A}_b^+\ \mathcal{A}_b^-\ \mathcal{E}_b\right)^T$. The dispersion relation is then obtained by requiring the matrix $\mathcal{M}$ to be singular. Although it cannot be handled analytically, this dispersion relation can easily be solved numerically, producing the semi-analytical solution to the problem in the infinitely thin flame limit.

#### 4.2.3. *Results*

Figure 5 displays the frequencies of the first three modes of the academic configuration II for $L=1$ m, $T_0^{\rm in}=300$ K, $T_0^{\rm out}=1200$ K and $p_{\rm in}=101325$ Pa; the flame position and thickness are $x_f=L/2$ and $\delta_f\simeq 0.047\ L$ respectively. Note that similar results are observed with different values of $x_f$ and $\delta_f$ although the Mach number effect on a particular mode may depend on these parameters. The case without unsteady combustion ($\hat{q}=0$) is considered first. In this case, no acoustic amplification/damping is generated by the flame if the mean flow is at rest. Moreover, with the boundary conditions chosen, the zero Mach number inlet/outlet acoustic flux $p_1u_1$ is zero at each instant. As a consequence, all the frequencies of oscillation are purely real when the mean flow is at rest (see $\triangle$ in Fig. 5). Note that the numerical results depicted here are in good agreement with the analytical solution available for zero Mach number in the case $T_0^{\rm out}/T_0^{\rm in}=4$ and $x_f=L/2$ [58]: 136.04 Hz, 347.19 Hz and 558.34 Hz for the first three modes respectively. Fig. 5 further shows that mean velocity effects are significant even for small Mach number values (see $\circ$ in Fig. 5); the imaginary part of the eigenmodes is clearly negative as soon as $M_0^{\rm in}>0.01$. Moreover, it becomes more and more negative with increasing inlet Mach number and large damping rates are obtained for $M_0^{\rm in}=0.15$, with imaginary frequency of $-53$ Hz, $-35$ Hz and $-37$ Hz for the first three modes respectively. Note that the real frequency shift between $M_0^{\rm in}=0$ and $M_0^{\rm in}=0.15$ is also not negligible for modes 1 and 2 ($-12$ Hz and $-24$ Hz, approx 9 % and 7 %) although much smaller for the third mode ($-6$ Hz, approx. 1 %). The same trends is obtained in the infinitely thin flame limit (see $\bullet$ in Fig. 5). The infinitely thin flame assumption either under-estimates (first mode) or over-estimates (third mode) the Mach number effects. The independence of the second

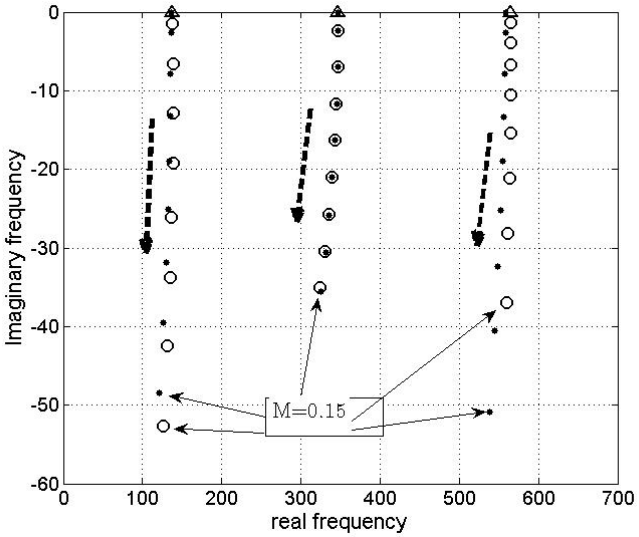


FIGURE 5. Location of the first three modes of the academic configuration II for different values of the inlet Mach number $M_0^{\text{in}}$. $\triangle$ : results from method **M2** for $M_0^{\text{in}} = 0$; $\circ$ : results from method **M1** for $M_0^{\text{in}} = 0.01$ to 0.15 with an increment of 0.02; $\bullet$ : semi-analytical solution from Eq. 4.5. Thick dashed arrows indicate increasing Mach numbers.

mode on the flame thickness is most probably due to the fact that the flame is located at a velocity node (first family of modes in [58]) for this mode. This observation is affirmed by other calculations: using the same setup, but placing the flame at $x_f = L/4$, the flame position coincides with a velocity node of the third mode. In this case, the agreement between semi-analytical results and those obtained with method **M1** is best for the third mode.

The structure of the first mode is depicted in Fig. 6 for different Mach number values. Even though acoustic and entropy waves are decoupled when the mean flow is at rest, entropy fluctuations are present in the flame region when $M_0^{\text{in}} = 0$, since in this case $j\omega\hat{s} = \hat{u}(ds_0/dx - r\hat{q}/p_0)$ (see Eq. 2.21) with $u_0 = 0$). Note that because of the homogeneous inlet condition, $\hat{s}(x = 0) = 0$, no entropy fluctuations are present until the flame can interact with the acoustic field. When the Mach number is not zero, entropy fluctuations are convected downstream of the flame so that, although the mean flow is isentropic, the equations of pure acoustics are no longer valid (strictly speaking) for $x > x_f + \delta_f/2$; indeed $\hat{p} \neq c_0^2\hat{\rho}$ when $\hat{s} \neq 0$. Downstream of the flame, the complex entropy amplitude is represented by Eq. 2.26; for damped modes, the imaginary part of the frequency $\omega$ is negative and the amplitude of $\hat{s}$ is a increasing function of $x$, as depicted in Fig. 6.

The numerical results are further tested/analyzed by constructing the acoustic and entropy pre-exponential factors $\mathcal{A}^+$, $\mathcal{A}^-$ and $\mathcal{E}$ as defined in Eqs. 2.23, 2.25 and 2.26. Since the mean flow is isentropic before and after the flame location, these quantities should be constant in these regions. The pressure, velocity and entropy fluctuations corresponding to the first mode have been combined as follows in order to construct the waves pre-exponential factors:

$$\mathcal{A}^+ = \frac{1}{2}\left(\hat{p}(x) + \rho_0 c_0 \hat{u}(x)\right) exp\left(-jk^+x\right)$$
$$\mathcal{A}^- = \frac{1}{2}\left(\hat{p}(x) - \rho_0 c_0 \hat{u}(x)\right) exp\left(jk^-x\right)$$

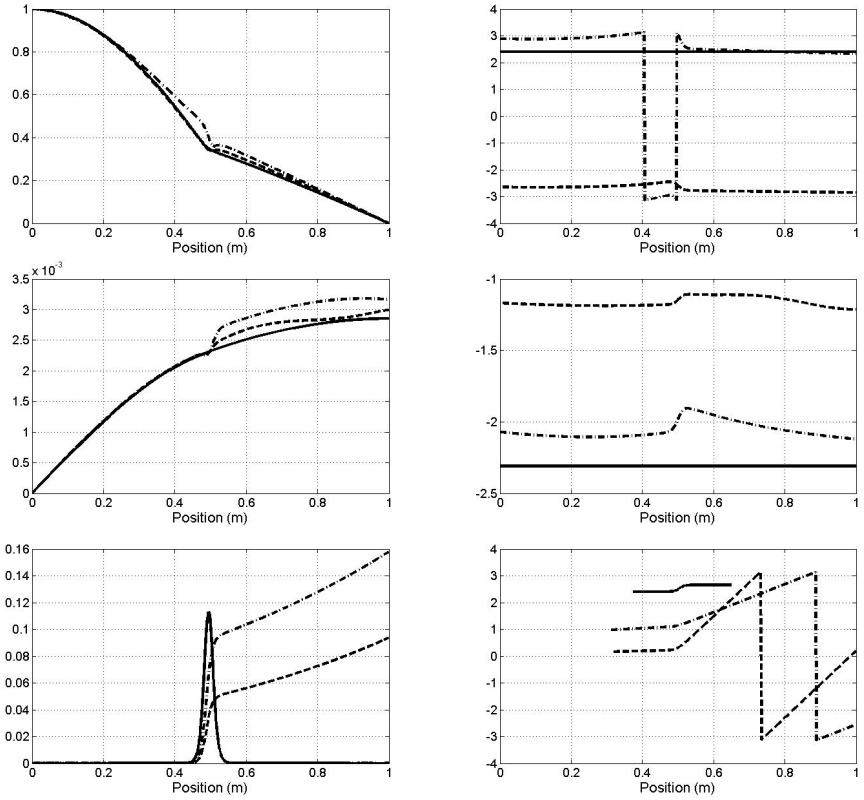


FIGURE 6. Structure of the first mode as obtained by Method **M1**. The amplitude (left column) and the phase (right column) of the complex amplitude of the pressure (top row), velocity (middle row) and entropy (bottom row) fluctuations are displayed. —— : $M_0^{\rm in} = 0$, $f \approx 137$ Hz; – – – : $M_0^{\rm in} = 0.05$, $f \approx 139 - 13i$ Hz; —·— : $M_0^{\rm in} = 0.11$, $f \approx 134 - 34i$ Hz. Normalization is $\hat{p}(x = 0) = 1$.

$$\mathcal{E} = \hat{s}(x) exp\,(-jk_s x) \tag{4.7}$$

The resulting values for small to medium Mach number values are depicted in Fig. 7. In all cases, the constant behavior expected upstream and downstream of the flame region is well recovered. Note that the entropy factor has been non-dimensionalized by $C_v|\mathcal{A}^+(x = 0)|/M_0^{\rm in} p_0^{\rm in}$ to reflect the fact that entropy is convected at the mean flow velocity. In the zero Mach number limit, the scaled entropy pre-exponential factor is negligible and the forward and backward acoustic coefficient share the same amplitude as imposed by the inlet/outlet boundary conditions. Since no entropy fluctuation is injected into the domain, the acoustic factor ratio $\mathcal{A}^-/\mathcal{A}^+$ is unity in the upstream part of the flow even for non zero Mach number values, consistently with the velocity imposed condition at the inlet. In the flame region, the mean flow is not isentropic so that the pre-exponential factors computed from Eqs. 4.7 cannot be interpreted in terms of waves. Still, the mean entropy evolves in this region and part of the acoustic energy is converted into entropy fluctuations. Downstream of the flame, the balance between the forward and backward acoustic waves is modified even if the zero acoustic pressure condition is imposed at the outlet. From Fig. 7, the $|\mathcal{A}^-/\mathcal{A}^+|$ ratio increases with the Mach number: it is close to 1, 1.3, 1.9 and 9.7 for $M_0^{\rm in} = 0$, 0.05, 0.11 and 0.2 respectively. Those large values of the acoustic pre-exponential factor ratio should not be misinterpreted, viz. they do

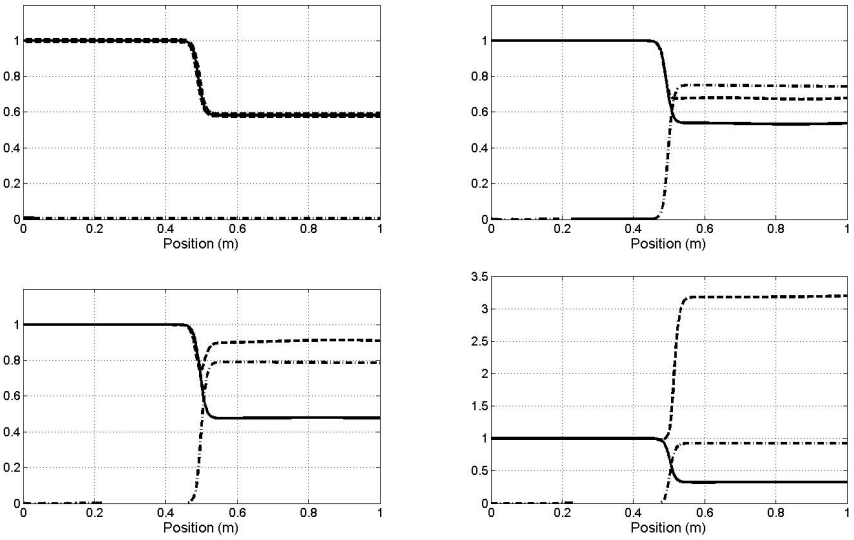


FIGURE 7. Pre-exponential factors for the forward acoustic wave $\mathcal{A}^+$ (——), backward acoustic wave $\mathcal{A}^-$ (- - -) and entropy wave $\mathcal{E}$ (—·—) normalized by $|\mathcal{A}^+(x=0)|$. Top left: $M_0^{\text{in}} = 0$, $f \approx 137$ Hz; Top right: $M_0^{\text{in}} = 0.05$, $f \approx 139 - 13i$ Hz; Bottom left: $M_0^{\text{in}} = 0.11$, $f \approx 134 - 34i$ Hz; Bottom right: $M_0^{\text{in}} = 0.2$, $f \approx 92 - 92i$ Hz. The entropy-to-acoustic pre-exponential factor ratio is further scaled by $C_v/M_0^{\text{in}} p_0^{\text{in}}$.

not correspond to acoustic energy entering the flow domain from the outlet section. Actually, the acoustic flux at $x = L$ (averaged over one cycle of oscillation and scaled by its counterpart at $x = 0$) is always positive, viz. 1, 1.47, 1.70 and 2.35 for $M_0^{\text{in}} = 0$, 0.05, 0.11 and 0.2 respectively, indicating increasing acoustic loss at the outlet. Here the acoustic flux has been computed as the time average of $(p_1 + \rho_0 u_0 u_1)(u_1 + p_1 u_0/\rho_0 c_0^2)$, as it is appropriate for moving media [59, 60]. Note also that the values obtained for $|\mathcal{A}^-/\mathcal{A}^+|$ are in good agreement with the theoretical assessment that can be derived under the isentropic mean flow assumption. In this case, the wave decomposition Eq. 2.23 together with the pressure imposed condition $\hat{p} = 0$ at $x = L$ leads to $|\mathcal{A}^-/\mathcal{A}^+|_b = \exp\left(-2\omega_i L/c_0(1 - M_b^2)\right)$. Defining the outlet reflexion coefficient as the wave amplitude ratio at $x = L$, viz. $R = \mathcal{A}^- \exp(-jk^- L) / [\mathcal{A}^+ \exp(+k^+ L)]$, one recovers $|R| = 1$, consistently with the zero pressure boundary condition.

When the unsteady flame contribution is accounted for, e.g. by using a $n - \tau$ type of model, the situation becomes more complex since the zero Mach number modes can be either stable or unstable depending on the phase between the acoustic pressure and the unsteady heat release. Only a global view of the potential effects of the mean flow is provided in the remaining of this section, a more detailed analysis being offered in section 4.3 for a particular mode. To this end, a parametric study has been conducted for the second mode of configuration II, the interaction index and time delay taking the values $0, 1, 2, 3, 4, 5$ and $0, 0.2, 0.4, ..., 2.4, 2.6$ ms respectively. In order to save computational time and because Fig. 5 showed a good agreement between the semi-analytical approach of [33] and the numerical results, the parametric study is based on solving Eq. 4.4 for each values of the $n - \tau$ parameters.

The results are shown in Fig. 8 which displays the frequency shifts (defined as the

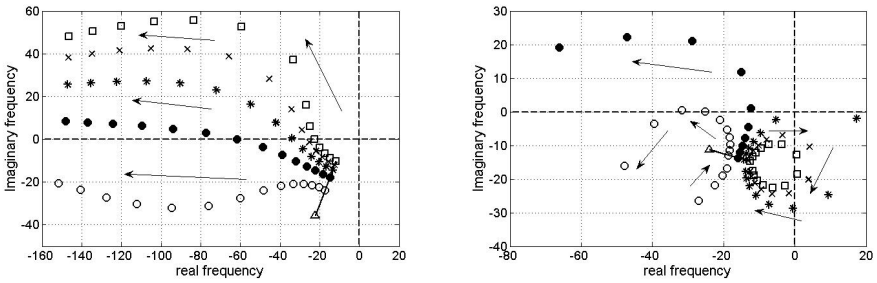


FIGURE 8. Frequency shifts at $M_0^{\text{in}} = 0.15$ for mode 2 of Configuration II. Each type of symbol represents a particular value of the interaction index. $\triangle : n = 0$, $\circ : n = 1$, $\bullet : n = 2$, $\star$: $n = 3$, $\times$: $n = 4$, $\square : n = 5$. For each value of $n$, the frequency shifts corresponding to several values of the time delay are displayed, from $\tau = 0$ to 2.6 ms, with an increment of 0.2 ms. The arrows indicate increasing time delays and the solid lines corresponds to zero time delay. The frequency is real valued in all cases when $M_0^{\text{in}} = 0$ and equals 347.19 Hz. Left: Simple BC; Right: Convective BC.

difference between the frequencies at $M_0^{\text{in}} = 0.15$ and $M_0^{\text{in}} = 0$) for each value of the flame response $n-\tau$. Two different sets of boundary conditions have been considered: the left plot corresponds to the simple conditions $\hat{u} = 0$ at $x = 0$ and $\hat{p} = 0$ at $x = L$ (Simple BC) while the right plot corresponds to $\hat{u} + \hat{p}u_0/\rho_0 c_0^2 = 0$ at $x = 0$ and $\hat{p} + \rho_0 u_0 \hat{u} = 0$ at $x = L$ (Convective BC). This second set of boundary conditions allows to set the acoustic flux at the boundaries to zero for the case of non zero Mach number mean flow [59, 60]. In terms of reduced impedance, these boundary conditions read $Z_u = \infty$; $Z_b = 0$ and $Z_u = -1/M_u$; $Z_b = -M_b$ respectively (see Eq. 4.5 for the use of $Z_u$ and $Z_b$ in the semi-analytical approach).

In both cases, the frequency shift due to the mean flow effects can hardly be guessed from a zero Mach number calculation. Indeed, the amplitude of the frequency change depends strongly on the nature of the flame-acoustic coupling (values of $n - \tau$) and thus on the mode considered. For the particular mode depicted in Fig. 8, it goes from less than 10 Hz to approx. 150 Hz, depending on the flame response and boundary condition characteristics. When Simple BC are used, the imaginary frequency shift can be either positive or negative, with a trend to be positive for large values of the interaction index. As a result, including the mean flow effects can make this particular mode either stable ($n = 1$ or $n = 2$ with $\tau < 1.4$ ms) or unstable (e.g.: $n = 5$ with $\tau > 0.8$ ms). Regarding the frequency of oscillation, the shift is always negative, consistently with the findings of section 4.1, but with a stronger amplitude: for large values of the time delay, the real frequency is decreased by one third when passing from $M_0^{\text{in}} = 0$ to $M_0^{\text{in}} = 0.15$. Overall, the frequency shifts are smaller when the Convective BC are used instead of the Simple BC. Moreover, including the non zero Mach number effects tends to stabilize the mode in almost all the cases, except for $n = 2$ and $\tau > 1$ ms. The real frequency shift remains mostly negative but smaller than in the Simple BC case. Gathering the results from the two sets of boundary conditions, only the first quadrant is never reached (positive real and imaginary frequency shifts) while the second and third quadrants (negative real frequency shift) are the most often reached. These results strongly suggest that zero Mach number thermo-acoustic analysis is not always enough to gain a clear view of the stability map of a combustor and that extension to non-zero Mach number mean flow formulation might be useful/necessary in some cases.

### 4.3. *Energy analysis*

In order to evaluate the origin of the differences between zero and non-zero Mach number mean flows, an analysis of the disturbance energy budget is carried out for configuration II. Since the mean flow in not isentropic, the acoustic and entropy modes of fluctuations interact and the energy analysis cannot rely on the acoustic energy only. Instead, the energy corollary proposed by Myers [27] and extended by Karimi et al. [61] to include combustion terms is used in this section. In the case of a 1D inviscid flow, this corollary can be written in the form:

$$\frac{\partial E_2}{\partial t} + \frac{\partial W_2}{\partial x} = D_2 \tag{4.8}$$

where $E_2$ is the first-order disturbance energy density defined as:

$$E_2 = \frac{p_1^2}{2\rho_0 c_0^2} + \frac{\rho_0 u_1^2}{2} + \rho_1 u_0 u_1 + \frac{\rho_0 T_0 s_1^2}{2c_{p_0}}, \tag{4.9}$$

$W_2$ is the first-order disturbance energy flux vector given by:

$$W_2 = (p_1 + \rho_0 u_0 u_1)(u_1 + \rho_1 u_0/\rho_0) + \rho_0 u_0 T_1 s_1 \tag{4.10}$$

and the source term $D_2$ reads:

$$D_2 = -s_1\rho_1 u_0 \frac{dT_0}{dx} - s_1\rho_0 u_1 \frac{dT_0}{dx} + s_1\rho_0 u_0 \frac{dT_1}{dx} + T_1\left(\frac{q_1}{T_0} - \frac{q_0 T_1}{T_0^2}\right) \tag{4.11}$$

It is obvious from the above expressions that even in 1D, keeping the mean velocity terms makes the situation much more complex (14 terms required to define $E_2$, $W_2$ and $D_2$ instead of 6 under the zero Mach number assumption). Using the results obtained with method **M1** (viz. using the LEE-Q1D tool of section 3.3 to solve the eigenvalue problem associated to the 1D Linearized Euler Equations discretized over $0 \leq x \leq L$), the time-dependent pressure fluctuation (or any other fluctuating quantity) associated to any thermo-acoustic mode can be computed by $p_1(x,t) = \Re\left(\hat{p}(x)exp(-j\omega t)\right)$. Testing the numerical solutions against Eq. 4.8 allows to **a)** demonstrate the accuracy of the numerical results and **b)** find out which terms in $W_2$ and $D_2$ are key ingredients to the time evolution of the disturbance energy $E_2$. The numerical setup is identical to the one in section 4.2.3 except for the flame thickness which is now $\delta_f \simeq 0.15\ L$. Moreover, the flame is no longer considered steady and the unsteady heat release is modeled as in Eq. 2.42, the local interaction index being given as :

$$\begin{aligned} &n_u(x) = \frac{n}{\delta_f} \times \frac{u_0^{\text{in}}}{q_{\text{tot}}} \times \frac{\gamma p_0}{\gamma - 1}, \quad \text{if} \quad x_f - \delta_f/2 < x < x_f + \delta_f/2, \\ &n_u(x) = 0 \quad \text{elsewhere}, \end{aligned} \tag{4.12}$$

where $q_{\text{tot}}$ is the total mean heat release in the domain and $n$ is the global interaction index of Eq. 2.40. We may note that for $\delta_f \longrightarrow 0$, Eq. 4.12 produces results equivalent to the thin flame model where the combustion process is restricted to the interface between the burnt and the unburnt gas [29]. The value $n = 5$ has been selected to obtain significant unsteady combustion effects on the thermo-acoustic modes while the time delay has been fixed to the constant value $\tau = 1$ ms.

The budget of Eq. 4.8 has been computed for two Mach number values, namely $M_0^{\text{in}} = 0$ and $M_0^{\text{in}} = 0.1$ and for the same two sets of boundary conditions as in Fig. 8, namely $\hat{u} = 0$ at $x = 0$; $\hat{p} = 0$ at $x = L$ (Simple BC) and $\hat{u} + \hat{p}u_0/\rho_0 c_0^2 = 0$ at $x = 0$; $\hat{p} + \rho_0 u_0 \hat{u} = 0$ at $x = L$ (Convective BC). One may note that in the case where the fluctuations are

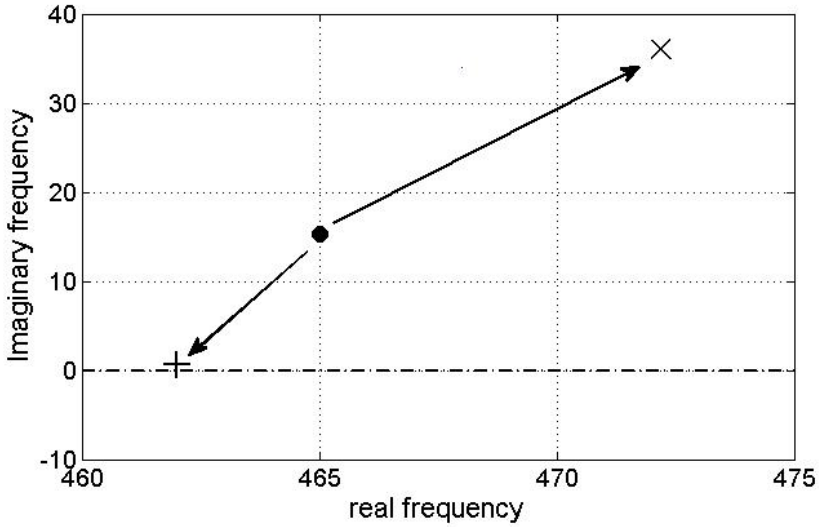


FIGURE 9. Position of the second mode of configuration II in the complex plane, for $x_f = L/2$, $\delta_f = 0.15\ L$, $n = 5$ and $\tau = 1$ ms. $\bullet$ : $M_0^{\rm in} = 0$ - $f = 465 + 15i$; $+$ : $M_0^{\rm in} = 0.1$ and Simple BC - $f = 472 + 36i$; $\times$: $M_0^{\rm in} = 0.1$ and Convective BC - $f = 462 + 0.7i$. The arrows show the displacement of the mode when $M_0^{\rm in}$ goes from 0 to 0.1

isentropic ($s_1 = 0$), the classical relationship $p_1 = c_0^2\rho_1$ holds and the energy flux $W_2$ becomes the acoustic flux as defined by Cantrell and Hart [59], Candel [60] in the case of a medium not at rest, viz. $(p_1 + \rho_0 u_0 u_1)(u_1 + p_1 u_0/\rho_0 c_0^2)$. Thus the Convective BC sets the energy flux to zero only in the case where the disturbances are isentropic. The Simple BC does the same in the restrictive case where the mean flow is at rest. The displacement of the mode for which the energy analysis is performed (the second mode of the setup) is shown in Fig. 9 when $M_0^{\rm in}$ increases from 0 to 0.1. Note that the mode is unstable in the zero Mach number case and that the mean flow effect depends on the boundary conditions. The mode becomes more unstable when the Simple BC are used whereas it becomes marginally unstable when the Convective BC are prescribed.

Eq. 4.8 is a direct consequence of the Linearized Euler Equation and thus it holds at each location and time. However, it is convenient to consider integrated versions of this equation in order to get insights about the different contributions. Since we restrict ourselves to the linear approximation, the instantaneous value of the disturbance energy is not as important as its evolution after one period of oscillation: if $E_2$ at time $t + T$ is greater than $E_2$ at time $t$, with $T = 1/f_r$, one may conclude that the mode is unstable since it contains more and more energy. Integrating Eq. 4.8 over one period of oscillation, one obtains the following exact equation:

$$E_2{}^{t=T} - E_2^{t=0} + \frac{d< W_2 >}{dx} - < D_2 >= 0, \tag{4.13}$$

where $< >$ stands for the time integration from $t = 0$ to $t = T$. The numerical results obtained for the three modes depicted in Fig. 9 have been post-processed and tested against Eq. 4.13 in Fig. 10. Note the scaling is such that $\max_x (< D_2 >) = 1$ and that different scales have been used for the bottom right plot. The type of boundary condition is not specified for $M_0^{\rm in} = 0$ since the Convective and Simple BCs are equivalent in this case. In all the cases considered, the computed LHS of Eq. 4.13 is very small compared to unity (of order 1 %, see bottom right), meaning that the results obtained are free of

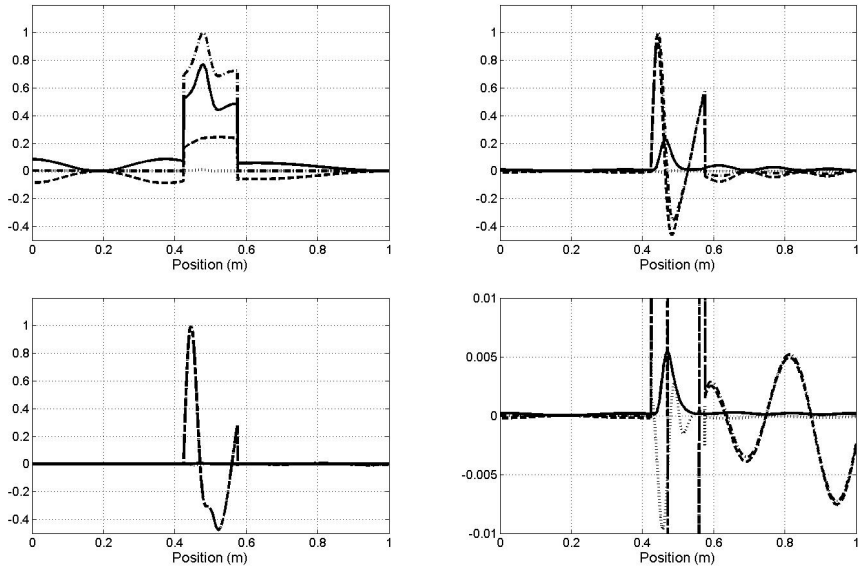


FIGURE 10. Spatial evolution of the terms in Eq. 4.13. Top left: $M_0^{\text{in}} = 0$; Top right: $M_0^{\text{in}} = 0.1$ and Simple BC; Bottom left: $M_0^{\text{in}} = 0.1$ and Convective BC; Bottom right: same as Bottom left but larger scale. —— : ${E_2}^{t=T} - E_2^{t=0}$, - - - : $d < W_2 > /dx$, —·— : $< D_2 >$, ····· : LHS of Eq. 4.13. All the terms are scaled by the maximum of $< D_2 >$ over space.

significant numerical errors. In the zero Mach number case (Top left in Fig. 10), the three terms have the same order of magnitude but the $E_2^{t=T} - E_2^{t=0}$ and $< D_2 >$ terms are always positive whereas the flux term $d< W_2 >/dx$ oscillates. When the Mach number equals 0.1, the source term oscillates over the domain, meaning that the unsteady flame feeds the disturbances at some locations and pumps energy at others. Such an effect can hardly be reproduced when the compact flame approximation is used. In the case where the Convective BC are used, the mode is virtually marginal; this explains why the $E_2^{t=T} - E_2^{t=0}$ term is so small in the bottom plots. The relative amplitude of this term is also smaller in the top right plot ($M_0^{\text{in}} = 0.1$ and Simple BC) than in the zero Mach number case. Since with the Simple BC the mode becomes more unstable when the Mach number increases (see Fig. 9), this is an effect of the oscillatory behavior of the $< D_2 >$ term (the scaling is based on the maximum value of $< D_2 >$ but the growth rate depends on the space integrated version of this quantity).

Integrating Eq. 4.13 further in space one obtains:

$$\overline{{E_2}^{t=T}} + \left[\overline{< W_2 >}\right]_{x=0}^{x=L} - \overline{< D_2 >} = 1, \tag{4.14}$$

where $\bar{\cdot}$ stands for the integral from $x = 0$ to $L$, $\left[\overline{< W_2 >}\right]_{x=0}^{x=L}$ is $\overline{< W_2 >}_{x=L} - \overline{< W_2 >}_{x=0}$ and the scaling is now such that $\overline{E_2^{t=0}} = 1$. The different terms involved in this exact equation are gathered in Table 4 for the three modes depicted in Fig. 9. With the retained scaling, the $\overline{E_2^{t=T}}$ entries are directly related to the growth rate of the modes and one can easily show that $\overline{E_2^{t=T}} = \exp(2\omega_i T)$, in agreement with the frequencies displayed in the table. One should also note that the disturbance energy is mostly of entropic nature, the relative amplitude of the acoustic energy (the first three terms in Eq. 4.9) being 36 %, 26 % and 32 % for the three cases reported (values not gathered in Table 4). When the Mach number is zero, both Simple or Convective BC ensure zero acoustic flux at the

| Case | $f$ (Hz) | $\overline{E_2^{t=T}}$ | $\overline{\left[< W_2 >\right]_{x=0}^{x=L}}$ | $\overline{< D_2 >}$ | LHS of Eq. 4.14 |
|---|---|---|---|---|---|
| $M_0^{\text{in}} = 0$ | $465.0 + 15.3\ j$ | 1.514 | 0 | 0.513 | 1.001 |
| $M_0^{\text{in}} = 0.1$ Simple BC | $472.2 + 36.0\ j$ | 2.609 | 0.363 | 2.002 | 0.974 |
| $M_0^{\text{in}} = 0.1$ Convective BC | $462.0 + 0.7\ j$ | 1.019 | 0.083 | 0.118 | 0.984 |

TABLE 4. Contributions of the separate terms of Eq. 4.14. Scaling is such that $\overline{E_2^{t=0}} = 1$.

| Case | $D_{2,1}$ $-s_1\rho_1 u_0 \frac{dT_0}{dx}$ | $D_{2,2}$ $-s_1\rho_0 u_1 \frac{dT_0}{dx}$ | $D_{2,3}$ $s_1\rho_0 u_0 \frac{\partial T_1}{\partial x}$ | $D_{2,4}$ $T_1 \frac{q_1}{T_0}$ | $D_{2,5}$ $-q_0 \frac{T_1^2}{T_0^2}$ | $\overline{< D_2 >}$ |
|---|---|---|---|---|---|---|
| $M_0^{\text{in}} = 0$ | 0 | 0.132 | 0 | 0.381 | 0 | 0.513 |
| $M_0^{\text{in}} = 0.1$ Simple BC | 0.868 | −0.055 | 0.919 | 1.938 | −1.668 | 2.002 |
| $M_0^{\text{in}} = 0.1$ Convective BC | 1.114 | 0.514 | 0.974 | −0.582 | −1.902 | 0.118 |

TABLE 5. Contributions to Eq. 4.14 of the five terms defining the source term $D_2$ in Eq. 4.11. The last column recalls the values of $\overline{< D_2 >}$ already given in Table 4 and corresponds to the sum of the entries $D_{2,1}$, ..., $D_{2,5}$.

inlet/outlet and since entropy fluctuations cannot be convected, the boundary term is zero. As a consequence, the growth rate is just and only related to the positive source term. In the second case considered (Simple BC and $M_0^{\text{in}} = 0.1$), the boundary term $\overline{\left[< W_2 >\right]_{x=0}^{x=L}}$ contributes significantly since 36 % of the energy initialy present in the domain is lost by the boundaries. This amount drops down to approx. 8 % when the Convective BC are used, consistentely with the fact that the acoustic flux is zeroed by this set of conditions but not by the Simple ones. Thus the mode with the Convective BC is more stable (less unstable) than its Simple BC counterpart although it loses less energy trough the boundaries per period of oscillation. This is due to the fact that the source term in Eq. 4.14 is much larger when Simple BC are used: in this case, more than twice the initial amount of energy is extracted from the mean flow and/or the flame whereas less than 12 % of this same amount is produced when the Convective BC are used. The contributions to the source terms are gathered in table 5 for the different cases considered. In the zero Mach number case, the major contributor is the temperature-heat release correlation (the $D_{2,4}$ term in Table 5) which is the counterpart

to the classical Rayleigh term when entropy fluctuations are included into the disturbance energy [62]. The other contributor (the $D_{2,2}$ term) describes how the overall fluctuation energy increases when a negative fluctuation of entropy ($s_1 < 0$, viz. $-s_1 > 0$) is convected toward region with larger mean entropy ($u_1 dT_0/dx > 0$). When using Simple BC to compute the $M_0^{\text{in}} = 0.1$ case, Table 5 indicates that the flame related source terms ($D_{2,4}$ and $D_{2,5}$) compensate each other and eventually produce the same amount of energy as in the $M_0^{\text{in}} = 0$ case, viz. roughly 30 % of the initial energy $\overline{E_2^{t=0}}$. However, there are two other significant contributors when the Mach number is finite, namely $D_{2,1}$ and $D_{2,3}$ which globally produce more than 170 % of $\overline{E_2^{t=0}}$. Note that $D_{2,1}$ and $D_{2,2}$ can be combined to give $-s_1 m_1 dT_0/dx$ where $m_1$ is the fluctuation of flow rate; thus the physical interpretation given above for $D_{2,2}$ can also be applied to the sum of the first two terms $D_{2,1} + D_{2,2}$. This mechanism remains very efficient in producing fluctuating energy when the Convective BC is used instead of the Simple one. The $D_{2,3}$ term can be partly related to the convection by the mean flow of the variance of the temperature fluctuations (assuming $s_1 \propto T_1$). Its contribution is indeed positive and remains essentially unchanged (of order $90-100$ % of $\overline{E_2^{t=0}}$) when the boundary conditions are modified. However, changing the boundary condition modifies the temperature-heat release correlation so that the $D_{2,4}$ term pumps energy when the Convective BC are used. Since the contribution from the mean heat release $q_0$ is also negative (by construction, see the definition of $D_{2,5}$ in table 5), the flame has a strong stabilizing effect in this case. Finally, the flame ($D_{2,4}+D_{2,5}$) and mean velocity/temperature terms ($D_{2,1}+D_{2,2}+D_{2,3}$) compensate so that the overall contribution of the source terms is far less significant in the Convective BC case compared to the Simple BC one. This leads to the difference in the mode stability displayed in Fig. 9.

### 4.4. *Combined mean flow effects: Academic configuration III*

The objective of this section is more to compare the results from Methods **M1** and **M2** (as defined in section 4.1.2) when applied to an academic yet representative configuration rather than analyzing the causes for the Mach number effects observed. This is the reason why the energy analysis presented above is not conducted in this section although this could be done without major difficulties.

As shown in figure 11, the setup is a combination of configurations I and II of Figs. 2 and 4: it consists in a constant cross section duct of length $L_c$ with a 1D flame of characteristic thickness $\delta_f$ located at $x = x_f$ and connected to a nozzle of length $L - L_c$. Note that this configuration is similar to the one studied by Polifke et al. [34, 35]. The mean flow is assumed isentropic except in the flame region and is constructed from the temperature profile Eq. 4.3 in the combustion chamber and the Mach number distribution Eq. 4.1 in the isentropic nozzle. The mean flow is then entirely determined by the choice of three independent inlet quantities (for example $p_0^{\text{in}}$, $T_0^{\text{in}}$, $M_0^{\text{in}}$), the outlet Mach number $M_0^{\text{out}}$ and relevant geometrical parameters $\delta_f$, $x_f$, $L_c$, $x_{\text{throat}}$ and $L$. Typical values of actual configurations have been selected for the flow/geometrical parameters relevant to this configuration (see table 6). $T_u$ and $T_b$ are the unburnt and burnt gas temperature respectively and are used in Eq. 4.3 to define the static temperature profile in the combustion chamber. The corresponding mean profiles are depicted in Fig. 12. Note that according to the order of magnitude analysis of Nicoud et al. [29], the mean flow effects might be non negligible in this configuration when the inlet Mach number is small compared to $\delta_f/L \approx 0.14$. Thus, with $M_0^{\text{in}} = 0.05$, the zero Mach number assumption for the mean flow is susceptible to induce significant errors.

Methods **M1** and **M2** (as defined in section 4.1.2) are used to perform the thermo-

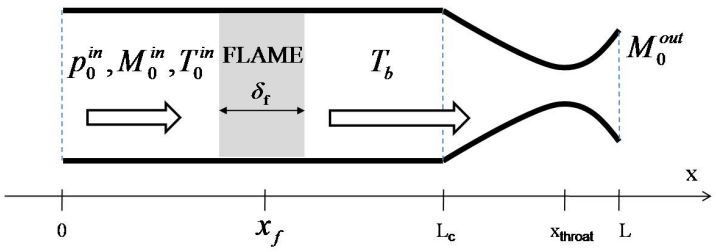


FIGURE 11. Principle of academic configuration III for illustrating the combined mean Mach number effects.

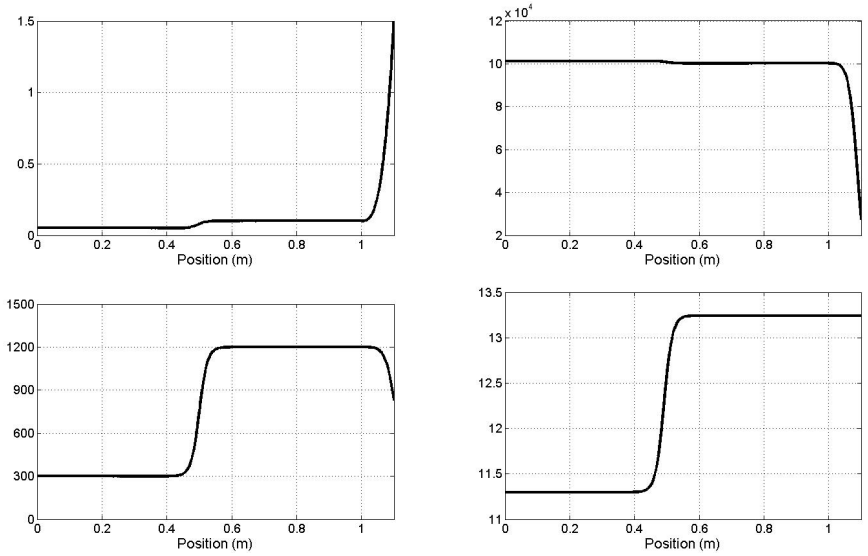


FIGURE 12. Mean flow fields for configuration III. Top left: Mach number; Top right: Static pressure (Pa); Bottom left: Static temperature (K); Bottom right: Entropy scaled by $C_v$.

| $L$ (m) | $L_c$ (m) | $x_{\text{throat}}$ (m) | $x_f$ (m) | $\delta_f$ (m) | $\gamma$ | $r$ (S.I) |
|---|---|---|---|---|---|---|
| 1.1 | 1.0 | 1.0863 | 0.5 | 0.15 | 1.4 | 287 |

| $p_0^{\text{in}}$ (Pa) | $T_0^{\text{in}} = T_u$ (K) | $T_b$ (K) | $M_0^{\text{in}}$ | $M_0^{\text{out}}$ | $x_{\text{ref}}$ (m) | $n$ | $\tau$ (s) |
|---|---|---|---|---|---|---|---|
| 101325 | 300 | 1200 | 0.05 | 1.5 | 0.42 | 3 | 0.001 |

TABLE 6. Main physical parameters used for configuration of Fig. 11.

acoustic analysis of the configuration described above in the case where unsteady combustion occurs. In the computations considered, the unsteady heat release is modeled as in section 4.3 (see Eq. 4.12) with the interaction index set to the value $n = 3$ (see table 6). Recall that this value corresponds to the low frequency limit of the interaction index when the burnt-to-unburnt temperature ratio equals 4, viz. $n \longrightarrow T_b/T_u - 1$ [58].

The inlet boundary conditions are as in section 4.2, viz. $\hat{u}(x = 0) = \hat{s}(x = 0) = 0$, whereas no outlet boundary condition is required for Method **M1** since the nozzle is choked; when Method **M2** is used, the equivalent acoustic impedance is computed from

the NOZZLE tool (see section 3.2) and applied at $x = L_c$ in the computation performed with the zero Mach number acoustic tool AVSP (see section 3.1).

In the following, the first mode computed from Methods **M1** and **M2** will be called mode $1_0$ and $1_{0.05}$ respectively, the index value referring to the inlet Mach number for these two computations. Under the conditions described in table 6 and Fig. 12, the frequency of mode $1_0$ is $f_0 = 234 + 32i$, whereas it is $f_{0.05} = 183 - 2i$ for mode $1_{0.05}$. In other words, the first mode of this configuration is found to be very unstable under the zero Mach number assumption for the mean flow and weakly stable when non zero Mach number effects are accounted for. Besides, the real frequency shift is significant since it reaches approx. 50 Hz or 25 % of the frequency of oscillation. Fig 13 shows that the structures of these two modes are very similar, at least in the cold region where entropy fluctuations are not present. Entropy fluctuations are generated in the region where the mean flow is not isentropic; those fluctuations are stationary in mode $1_0$ but are convected in mode $1_{0.05}$, as the phase of $\hat{s}$ indicates in Fig. 13. Note also that the velocity jump related to the unsteady combustion in the flame region is significantly larger in mode $1_{0.05}$ compared to mode $1_0$; this is most probably due to the fact that the entropy generation in the flame region is under-estimated when the mean flow is at rest. In this latter case, the mean heat release $q_0$ is null, zeroing two contributors to the entropy equation (third row in Eq. 2.21). This difference in the amount of entropy fluctuation induces a large change in the pressure phase in the flame region: from Fig. 13, it is $\phi_0^p \approx -2.4$ for mode $1_0$ and $\phi_{0.05}^p \approx -1$ for mode $1_{0.05}$. Upstream the flame, the two modes share the same velocity phase, especially near $x = 0.42$ m, the location of the reference point used in the local $n - \tau$ model to represent the unsteady heat release (denoting by $\phi_u$ the phase of the velocity at this location, Fig. 13 suggests $\phi_u \approx 1.5$). From the form of the local $n - \tau$ model, Eq. 2.42, the following approximations can be obtained for the phase of the unsteady heat release: $\phi_0^q = \phi_u + 2\pi \mathrm{Re}(f_0)\ \tau \approx 3$ for mode $1_0$ and $\phi_{0.05}^q = \phi_u + 2\pi \mathrm{Re}(f_{0.05})\ \tau \approx 2.7$ for mode $1_{0.05}$. Finally, the phase difference between heat release and pressure is approx. $\Delta\phi_0 \approx 3 - (-2.4) \approx 5.4$ for mode $1_0$ and $2.7 - (-1) \approx 3.7$ for mode $1_{0.05}$. In other words, Fig. 13 indicates that pressure and heat release fluctuations are in phase for mode $1_0$ (since $-\pi/2\ [2\pi] < \Delta\phi_0 < \pi/2\ [2\pi]$) and out of phase for mode $1_{0.05}$ (since $\pi/2\ [2\pi] < \Delta\phi_{0.05} < 3\pi/2\ [2\pi]$). According to the Rayleigh criterion [1], this means that mode $1_0$ is unstable (assuming that acoustic losses are too small to compensate for the energy feeding from the acoustic/flame coupling) and that mode $1_{0.05}$ is stable. This result is of course in agreement with the frequency values of these two modes ($\mathrm{Im}(f_0) > 0$, $\mathrm{Im}(f_{0.05}) < 0$); it also supports the idea that entropy generation/propagation is a key phenomenon that should be appropriately accounted for when performing thermo-acoustic analysis of non zero Mach number flows.

## 5. CONCLUSION

Several 1D or quasi-1D academic test cases have been considered to assess the origin and amount of the errors made when performing thermo-acoustic analysis under the zero Mach number assumption. Results from two different methods have been compared: the reference method consisted in solving the eigenvalue problem arising from the Linearized Euler Equations written in the frequency space; the other method consisted in using an Helmholtz solver for representing the small velocity regions, the high speed regions being represented by an equivalent acoustic impedance computed beforehand. Beside the

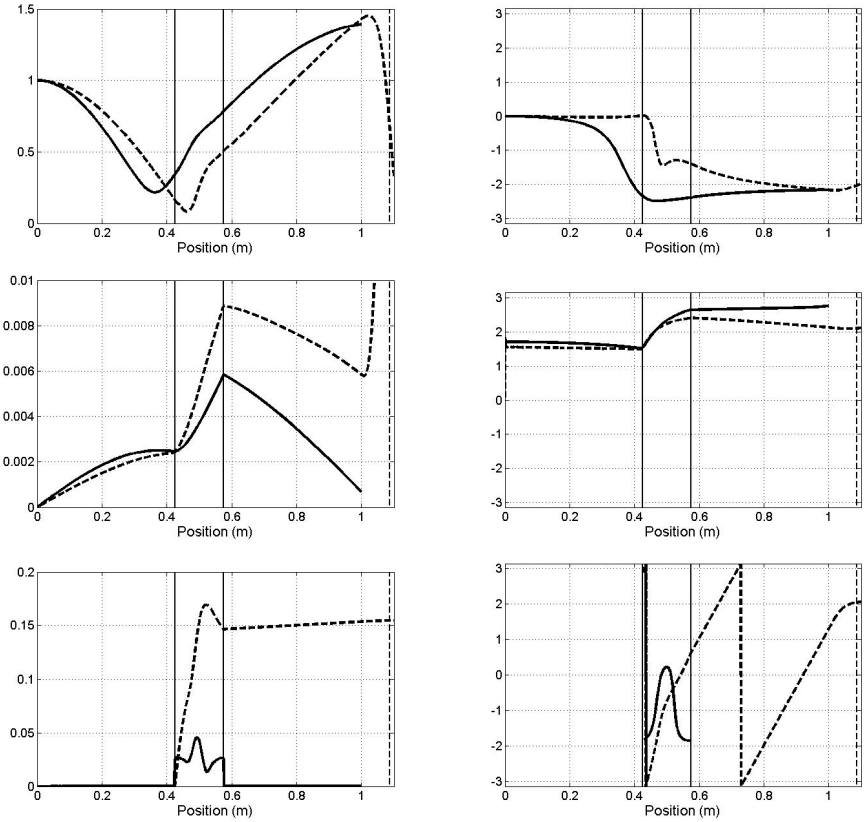


FIGURE 13. Structure of the modes $1_0$ and $1_{0.05}$. The amplitude (left column) and the phase (right column) of the complex amplitude of the pressure (top row), velocity (middle row) and entropy (bottom row) fluctuations are displayed. —— : mode $1_0$, $M_0^{\text{in}} = 0$; – – – : mode $1_{0.05}$, $M_0^{\text{in}} = 0.05$. Normalization is $\hat{p}(x = 0) = 1$. The two vertical solid lines denote the flame region; the vertical dashed line is the throat location.

expected frequency shift due to the change in the speed of propagation of the pressure waves, an important source of error is related to the interaction between the disturbances and the flame region. The budget of the disturbance energy equation shows that several source terms proportional to the mean velocity contribute as much as the classical pressure or temperature - heat release correlation ('Rayleigh' term). As a result, when the mean flow is assumed to be at rest, the amount of entropy fluctuations generated in the flame region is not well estimated; besides, the entropy fluctuations arising from the acoustic/flame interaction remain in their production zone since no convection occurs when the Mach number is zero. The absence of the entropy mode downstream of the flame region induces significant changes in the structure of the thermo-acoustic mode even for moderate Mach numbers. The analysis also illustrated that the net effect of the non zero Mach number terms strongly depends on the characteristics of the flame response to disturbances and also on the boundary conditions. For the academic (yet representative to practical combustors) configuration considered, the errors induced by the zero Mach number assumption for the mean flow are large enough to modify the stability of the first mode for an inlet Mach number as small as 0.05.

KW is grateful to the European Community for funding her PhD work under the

project AETHER (Contract No. FP6 - MRTN-CT-2006-035713). This work was also performed in the framework of the BRUCO project funded by the Fondation Nationale de Recherche pour l'Aéronautique et l'Espace. The authors also would like to thank the Centre Informatique National de l'Enseignement Supérieur for giving access to supercomputing facilities and E. Gullaud for providing the zero Mach number results from the AVSP code.

## Appendix A. Derivation of the quasi-1D equations

These equations are best derived, either in the physical or in the frequency space, by considering first the non-linearized flow equations 2.1-2.3 written in a conservative form:

$$\frac{\partial \rho}{\partial t} + \nabla \cdot \rho \mathbf{u} = 0, \tag{A 1}$$

$$\frac{\partial \rho \mathbf{u}}{\partial t} + \nabla \cdot (p\mathbf{I} + \rho \mathbf{u} \otimes \mathbf{u}) = 0, \tag{A 2}$$

$$\frac{\partial \rho s}{\partial t} + \nabla \cdot \rho \mathbf{u} s = \frac{q}{T}, \tag{A 3}$$

where $\mathbf{I}$ is the identity second order tensor. Let us first consider a quasi-1D flow domain $\Omega$ whose cross section area $\mathcal{S}$ is a slowly varying function of the principal axis of the domain, the $x$-direction say (see Fig. 1). Let us call $\Gamma$ the lateral boundary of $\Omega$ and $\partial\Omega$ its complete boundary. If one denotes by $\mathcal{S}_{\rm in}$ and $\mathcal{S}_{\rm out}$ the inlet and outlet cross sections of $\Omega$, it is obvious that $\partial\Omega = \Gamma \cup \mathcal{S}_{\rm in} \cup \mathcal{S}_{\rm out}$. Similarly, one may define $\Omega_1^2$ the subset of $\Omega$ defined by the intersection of $\Omega$ with the range $x_1 \leq x \leq x_2$ where $x_1$ and $x_2$ are such that $x_{\rm in} \leq x_1 < x_2 \leq x_{\rm out}$; the boundary of $\Omega_1^2$ is then $\partial\Omega_1^2 = \Gamma_1^2 \cup \mathcal{S}_1 \cup \mathcal{S}_2$ where obvious notations have been used. For any conserved variable $\phi$ whose transport equation reads:

$$\frac{\partial \rho \phi}{\partial t} + \nabla \cdot \mathcal{F}(\phi) = 0, \tag{A 4}$$

where $\mathcal{F}(\phi)$ is the flux of $\phi$, one may obtain the corresponding quasi-1D equation by first integrating Eq. A 4 over the volume $\Omega_1^2$. Since the volume of integration does not depend on time, one obtains:

$$\frac{\partial < \rho\phi >}{\partial t} + \int\int_{\Gamma_1^2} \mathcal{F}(\phi) \cdot \mathbf{n} d\Gamma_1^2 - \int\int_{\mathcal{S}(x_1)} \mathcal{F}_x(\phi) d\mathcal{S}(x_1) + \int\int_{\mathcal{S}(x_2)} \mathcal{F}_x(\phi) d\mathcal{S}(x_2) = 0, \tag{A 5}$$

where $< \rho\phi >$ is the volume integral of $\rho\phi$ and the divergence theorem has been used to express the integral of the divergence term in Eq. A 4; to this respect, $\mathbf{n}$ is the outward unit vector normal to $\partial\Omega_1^2$. With $\mathcal{F}_x$ the $x$-component of $\mathcal{F}$, the RHS of Eq. A 5 is obtained by recognizing that $\mathbf{n}$ equals $(1,0,0)$ and $(-1,0,0)$ over $\mathcal{S}(x_2)$ and $\mathcal{S}(x_1)$ respectively. The volume integral of $\rho\phi$ can be recast in :

$$< \rho\phi >= \int_{x_1}^{x_2} \left( \int\int_{\mathcal{S}(x)} \rho\phi d\mathcal{S}(x) \right) dx$$

so that it is useful to introduce the cross section averaging operator:

$$\overline{\psi}(x) = \frac{1}{\mathcal{S}(x)} \int\int_{\mathcal{S}(x)} \psi d\mathcal{S}(x),$$

which can be applied to any integrable physical quantity $\psi$ and where $\mathcal{S}(x)$ must be understood as the area of the cross section $\mathcal{S}$ at position $x$. Equation A 5 can then be written in a more compact form:

$$\frac{\partial \int_{x_1}^{x_2} \mathcal{S}(x) \overline{\rho\phi} dx}{\partial t} + \int\int_{\Gamma_1^2} \mathcal{F}(\phi) \cdot \mathbf{n} d\Gamma_1^2 - \mathcal{S}(x_1) \overline{\mathcal{F}_x}(x_1) + \mathcal{S}(x_2) \overline{\mathcal{F}_x}(x_2) = 0, \tag{A 6}$$

We now have the liberty to choose $x_1$ and $x_2$ in a convenient way; taking $x_1 = x$ and $x_2 = x + \Delta x$ where $\Delta x$ is an arbitrarily small increment, Eq. A 6 leads to:

$$\mathcal{S}\frac{\partial\overline{\rho\phi}}{\partial t} + \int_{\mathcal{C}} \mathcal{F}(\phi)\cdot\mathbf{n}_c d\mathcal{C} + \frac{\partial\mathcal{S}\overline{\mathcal{F}_x}}{\partial x} = 0, \tag{A 7}$$

where $\mathcal{C}$ is the contour defined as the intersection between $\Gamma$ and the plane orthogonal to the $x$-axis at position $x$. Note also that dependences on $x$ have been omitted for clarity and that $\mathbf{n}_c$ is the outward unit vector normal to $\mathcal{C}$ belonging to the $x$-plane.

Choosing either $\phi = 1$, $\phi = u$ or $\phi = s$, the integral term in Eq. A 7 contributes only when $d\mathcal{S}/dx \neq 0$ since $\mathcal{F}$ is either zero or aligned with the $x$-direction over the lateral boundary $\Gamma$. The following quasi-1D equations for mass, streamwise velocity and entropy can then be derived from Eq. A 7:

$$\frac{\partial\overline{\rho}}{\partial t} + \frac{\partial\overline{\rho u}}{\partial x} + \frac{\overline{\rho u}}{\mathcal{S}}\frac{\partial\mathcal{S}}{\partial x} = 0, \tag{A 8}$$

$$\frac{\partial\overline{\rho u}}{\partial t} + \frac{\partial\overline{p} + \overline{\rho u^2}}{\partial x} + \frac{\overline{\rho u^2}}{\mathcal{S}}\frac{\partial\mathcal{S}}{\partial x} = 0, \tag{A 9}$$

and

$$\frac{\partial\overline{\rho s}}{\partial t} + \frac{\partial\overline{\rho u s}}{\partial x} + \frac{\overline{\rho u s}}{\mathcal{S}}\frac{\partial\mathcal{S}}{\partial x} = \overline{\frac{q}{T}}, \tag{A 10}$$

Note that no assumption has been made so far, except that the flow takes place in a domain $\Omega$ such that the cross section area $\mathcal{S}$ can be taken as a function of $x$. We now introduce the quasi-1D approximation, neglecting the in-plane correlation terms, viz. assuming $\overline{\phi\psi} = \overline{\phi}\ \overline{\psi}$. Eqs. A 8-A 10 can then be combined to give the following set of quasi-1D equations written in non-conservative form:

$$\frac{\partial\overline{\rho}}{\partial t} + \overline{u}\frac{\partial\overline{\rho}}{\partial x} + \overline{\rho}\frac{\partial\overline{u}}{\partial x} + \frac{\overline{\rho}\ \overline{u}}{\mathcal{S}}\frac{\partial\mathcal{S}}{\partial x} = 0, \tag{A 11}$$

$$\overline{\rho}\frac{\partial\overline{u}}{\partial t} + \overline{\rho}\ \overline{u}\frac{\partial\overline{u}}{\partial x} = -\frac{\partial\overline{p}}{\partial x}, \tag{A 12}$$

$$\frac{\partial\overline{s}}{\partial t} + \overline{u}\frac{\partial\overline{s}}{\partial x} = \frac{r\overline{q}}{\overline{p}}, \tag{A 13}$$

Except for the equation of mass which now contains an extra term related to the geometry of the domain, the quasi-1D equations to be considered are essentially the 1D restriction of the 3D equations of motion 2.1-2.3. Omitting the $\bar{\cdot}$ operator for simplicity and introducing the decomposition of each variable into a steady component (subscript '0') and an unsteady, small amplitude fluctuating part (subscript '1'), one eventually obtains the quasi-1D set of linear differential equations given in the main text, Eqs. 2.18-2.20.

## References


1. Rayleigh, L. The explanation of certain acoustic phenomena. *Nature*, vol. July 18, pp. 319–321 (1878).
2. Putnam, A. A. *Combustion driven oscillations in industry.* American Elsevier, fuel and energy science series, j.m. beer edn. (1971).
3. Poinsot, T. and Candel, S. Interactions between acoustics and combustion. In *Acoustics 88.* (1988).
4. Culick, F. E. C. Combustion instabilities in liquid-fueled propulsion systems- An overview. In *AGARD 72B PEP meeting* (1987).

5. Lieuwen, T. and Yang, V. Combustion Instabilities in Gas Turbine Engines. Operational Experience, Fundamental Mechanisms and Modeling. In *Prog. in Astronautics and AeronauticsAIAA*, vol. 210 (2005).
6. Desjardins, P. E. and Frankel, S. H. Two dimensional Large Eddy Simulation of soot formation in the near field of a strongly radiating nonpremixed acetylene-air jet flame. *Combust. Flame*, vol. 119(1/2), pp. 121–133 (1999).
7. Murota, T. and Ohtsuka, M. Large-Eddy Simulations of Combustion Oscillation in Premixed Combustor. In *International Gas Turbine and Aeroengine Congress & Exposition, ASME Paper*, vol. 99-GT-274 (1999).
8. Caraeni, D., Bergstrom, C., and Fuchs, L. Modeling of Liquid Fuel Injection, Evaporation and Mixing in a Gas Turbine Burner Using Large Eddy Simulation. *Flow, Turb. and Combustion*, vol. 65, pp. 223–244 (2000).
9. Colin, O., Ducros, F., Veynante, D., and Poinsot, T. A thickened flame model for large eddy simulations of turbulent premixed combustion. *Phys. Fluids*, vol. 12(7), pp. 1843–1863 (2000).
10. Pierce, C. D. and Moin, P. Progress-variable approach for large eddy simulation of non-premixed turbulent combustion. *J. Fluid Mech.*, vol. 504, pp. 73–97 (2004).
11. Selle, L., Lartigue, G., Poinsot, T., Koch, R., Schildmacher, K.-U., Krebs, W., Prade, B., Kaufmann, P., and Veynante, D. Compressible Large-Eddy Simulation of turbulent combustion in complex geometry on unstructured meshes. *Combust. Flame*, vol. 137(4), pp. 489–505 (2004).
12. Pitsch, H. Large Eddy Simulation of Turbulent Combustion. *Ann. Rev. Fluid Mech.*, vol. 38, pp. 453–482 (2006).
13. Angelberger, C., Egolfopoulos, F., and Veynante, D. Large Eddy Simulations of chemical and acoustic effects on combustion instabilities. *Flow, Turb. and Combustion*, vol. 65(2), pp. 205–22 (2000).
14. Huang, Y. and Yang, V. Bifurcation of flame Structure in a Lean Premixed Swirl-Stabilized Combustor: Transition from Stable to Unstable Flame. *Combust. Flame*, vol. 136, pp. 383–389 (2004).
15. Roux, S., Lartigue, G., Poinsot, T., Meier, U., and Bérat, C. Studies of mean and unsteady flow in a swirled combustor using experiments, acoustic analysis and Large Eddy Simulations. *Combust. Flame*, vol. 141, pp. 40–54 (2005).
16. Schmitt, P., Poinsot, T. J., Schuermans, B., and Geigle, K. Large-eddy simulation and experimental study of heat transfer, nitric oxide emissions and combustion instability in a swirled turbulent high pressure burner. *J. Fluid Mech.*, vol. 570, pp. 17–46 (2007).
17. Poinsot, T. and Veynante, D. *Theoretical and numerical combustion.* R.T. Edwards (2001).
18. Stow, S. R. and Dowling, A. P. Thermoacoustic oscillations in an annular combustor. In *ASME Paper*. New Orleans, Louisiana (2001).
19. Stow, S. R. and Dowling, A. P. Modelling of circumferential modal coupling due to Helmholtz resonators. In *ASME Paper 2003-GT-38168*. Atlanta, Georgia, USA (2003).
20. Evesque, S. and Polifke, W. Low-Order Acoustic Modelling for Annular Combustors: Validation and Inclusion of Modal Coupling. In *International Gas Turbine and Aeroengine Congress & Exposition, ASME Paper*, vol. GT-2002-30064 (2002).
21. Evesque, S., Polifke, W., and Pankiewitz, C. Spinning and Azimuthally Standing Acoustic Modes in Annular Combustors. In *9th AIAA/CEAS Aeroacoustics Conference*, vol. AIAA paper 2003-3182 (2003).
22. Morgans, A. S. and Stow, S. R. Model-based control of combustion instabilities in

annular combustors. *Combust. Flame*, vol. 150(4), pp. 380–399 (2007).
23. Chu, B. T. On the energy transfer to small disturbances in fluid flow (Part I). *Acta Mechanica*, pp. 215–234 (1965).
24. Pankiewitz, C. and Sattelmayer, T. Time domain simulation of combustion instabilities in annular combustors. *ASME Journal of Engineering for Gas Turbines and Power*, vol. 125(3), pp. 677–685 (2003).
25. Rao, P. and Morris, P. Use of finite element methods in frequency domain aeroacoustics. *Am. Inst. Aeronaut. Astronaut. J.*, vol. 44(7), pp. 1643–1652 (2006).
26. Kovasznay, L. Turbulence in supersonic flow. *J. Aeronaut. Sci.*, vol. 20, pp. 657–674 (1953).
27. Myers, M. Transport of energy by disturbances in artitrary steady flows. *J. Fluid Mech.*, vol. 226, pp. 383–400 (1991).
28. Howe, M. S. *Acoustics of Fluid-Structure Interaction*. Cambridge University Press (1998).
29. Nicoud, F., Benoit, L., Sensiau, C., and Poinsot, T. Acoustic Modes in Combustors with Complex Impedances and Multidimensional Active Flames. *AIAA Journal*, vol. 45, pp. 426–441 (2007).
30. Martin, C., Benoit, L., Sommerer, Y., Nicoud, F., and Poinsot, T. LES and acoustic analysis of combustion instability in a staged turbulent swirled combustor. *AIAA Journal*, vol. 44(4), pp. 741–750 (2006).
31. Selle, L., Benoit, L., Poinsot, T., Nicoud, F., and Krebs, W. Joint use of Compressible Large-Eddy Simulation and Helmoltz solvers for the analysis of rotating modes in an industrial swirled burner. *Combust. Flame*, vol. 145(1-2), pp. 194–205 (2006).
32. Keller, J. J., Egli, W., and Hellat, J. Thermally induced low-frequency oscillations. *J. Appl. Math. Phys.*, vol. 36(12), pp. 250–274 (1985).
33. Dowling, A. P. The calculation of thermoacoustic oscillations. *J. Sound Vib.*, vol. 180(4), pp. 557–581 (1995).
34. Polifke, W., Paschereit, C., and Doebbeling, K. Suppression of combustion instabilities through destructive interference of acoustic and entropy waves. In *In 6th. Int. Conf. on Sound and Vibration, Copenhagen, Denmark* (1999).
35. Polifke, W., Paschereit, C., and Doebbeling, K. Constructive and Destructive Interference of Acoustic and Entropy Waves in a Premixed Combustor with a Choked Exit. *Int. J. Acoust. Vib.*, vol. 6, pp. 135–146 (2001).
36. Sattelmayer, T. Influence of the Combustor Aerodynamics On Combustion Instabilities from Equivalence Ratio Fluctuations. *J. Eng. Gas Turb. and Power*, vol. 125, pp. 11–19 (2003).
37. Lefebvre, A. H. *Gas Turbines Combustion*. Taylor & Francis (1999).
38. Marble, F. E. and Candel, S. Acoustic disturbances from gas nonuniformities convected through a nozzle. *J. Sound Vib.*, vol. 55, pp. 225–243 (1977).
39. Balasubramanian, K. and Sujith, R. I. Thermoacoustic instability in a Rijke tube: Non-normality and nonlinearity. *Phys. Fluids*, vol. 20(4), pp. 044103–11 (2008).
40. Trefethen, L., Trefethen, A., Reddy, S., and Driscoll, T. Hydrodynamic stability without eigenvalues. *Science*, vol. 261, pp. 578–584 (1993).
41. Balasubramanian, K. and Sujith, R. I. Non-normality and nonlinearity in combustion–acoustic interactions in diffusion flames,. *J. Fluid Mech.*, vol. 594(4), pp. 29–57 (2008).
42. Giauque, A., Poinsot, T., Brear, M., and Nicoud, F. Budget of disturbance energy in gaseous reacting flows. In *Proc. of the Summer Program*, pp. 285–297. Center for Turbulence Research, NASA Ames/Stanford Univ. (2006).
43. Cummings, A. Ducts with axial temperature gradients: an approximate solution for

sound transmission and generation. *J. Sound Vib.*, vol. 51, pp. 55–67 (1977).
44. Kapur, A., A.and Cummings and Mungur, P. Sound propagation in a combustion can with axial temperature and density gradients. *J. Sound Vib.*, vol. 25(1), pp. 129–138 (1972).
45. Peat, K. S. The tranfer matrix of a uniform duct with a linear temperature gradient. *J. Sound Vib.*, vol. 123, pp. 43–53 (1988).
46. Karthik, B., Kumar, B. M., and Sujith, R. I. Exact solutions to one-dimensional acoustics field with temperature gradient and mean flow. *J. Acous. Soc. Am.*, vol. 108(1), pp. 38–43 (2000).
47. Lieuwen, T. Modeling Premixed Combustion-Acoustic Wave Interactions: A Review. *J. Prop. Power*, vol. 19(5), pp. 765–781 (2003).
48. Schuller, T., Durox, D., and Candel, S. A unified model for the prediction of laminar flame transfer functions: comparisons between conical and V-flames dynamics. *Combust. Flame*, vol. 134, pp. 21–34 (2003).
49. Dowling, A. P. Nonlinear self-exited oscillations of a ducted flame. *J. Fluid Mech.*, vol. 346, pp. 271–290 (1997).
50. Lieuwen, T. and Zinn, B. T. The Role of Equivalence Ratio Oscillations In Driving Combustion Instabilities In Low NOx Gas Turbines. *Proc. Combust. Inst.*, vol. 27, pp. 1809–1816 (1998).
51. Sattelmayer, T. Influence of the combustor aerodynamics un combustion instabilities from equivalence ratio fluctuations. In *International Gas Turbine and Aeroengine Congress and Exhibition*. ASME Paper, Munich (2000).
52. Crocco, L. Aspects of combustion instability in liquid propellant rocket motors. Part I. *J. American Rocket Society*, vol. 21, pp. 163–178 (1951).
53. Crocco, L. Aspects of combustion instability in liquid propellant rocket motors. Part II. *J. American Rocket Society*, vol. 22, pp. 7–16 (1952).
54. Tisseur, F. and Meerbergen, K. The quadratic eigenvalue problem. *SIAM Review*, vol. 43, pp. 235–286 (2001).
55. Lehoucq, R. and Sorensen, D. ARPACK: Solution of Large Scale Eigenvalue Problems with Implicitly Restarted Arnoldi Methods. www.caam.rice.edu/software/ARPACK. User's guide (1997).
56. Sleijpen, G., Van der Vorst, H., and van Gijzen, M. Quadratic eigenproblems are no problem. *SIAM News*, vol. 29(7) (1996).
57. Sensiau, C., Nicoud, F., van Gijzen, M., and van Leeuwen, J. A comparison of solvers for quadratic eigenvalue problems from combustion. *Int. J. Numer. Meth. Fluids*, vol. 56, pp. 1481–1487 (2008).
58. Kaufmann, A., Nicoud, F., and Poinsot, T. Flow forcing techniques for numerical simulation of combustion instabilities. *Combust. Flame*, vol. 131, pp. 371–385 (2002).
59. Cantrell, R. and Hart, R. Interaction between sound and flow in acoustic cavities: mass, momentum and energy considerations. *J. Acous. Soc. Am.*, vol. 36, pp. 697–701 (1964).
60. Candel, S. Acoustic conservation principles, application to plane and modal propagation in nozzles and diffusers. *J. Sound Vib.*, vol. 41, pp. 207–232 (1975).
61. Karimi, N., Brear, M. J., and Moase, W. H. Acoustic and disturbance energy analysis of a flow with heat communication. *J. Fluid Mech.*, vol. 597, pp. 67–89 (2008).
62. Nicoud, F. and Poinsot, T. Thermoacoustic instabilities: should the Rayleigh criterion be extended to include entropy changes ? *Combust. Flame*, vol. 142, pp. 153–159 (2005).